

## 1

## Introduction: Progress of Thin Films and Coatings

Yujun Song<sup>1,2</sup>

<sup>1</sup>University of Science and Technology Beijing, Center for Modern Physics Technology, Applied Physics Department, School of Mathematics and Physics, 30 Xueyuan Road, Beijing 100083, China

<sup>2</sup>Zhejiang Key Laboratory for Pulsed Power Technology Translational Medicine, Hangzhou Ruidi Biotechnology Company, Hangzhou 310000, China

### 1.1 Introduction

As one cornerstone of advanced modern technologies, thin films and coatings have been expanding its scope into varieties of emerging research areas and developing rapidly to match the requirement from academics and industrials in the past decades. As elucidated in this book, thin films and coatings that are never dispensable for the development of modern science and technology will continuously play the key innovation driving force in the next generation of computing and information technology, new energy, biology and life science, new medicines, astronautics and aeronautics, geology and ocean engineering, military science, etc. Eventually pushed by the requirement of industrial sectors of countries, the successful application of this field depends intrinsically on the fundamental progress of the surface/interface science and the precision of the related mass fabrication technology. This may be the main reason for “the interface is the device” stated by Herbert Kroemer, the Nobel Prize winner in Physics in 2000 [1, 2] and for so many Nobel Prize winners in the fields relating to surface/interface science (e.g. 1930 Nobel Prize winner in Physics Chandrasekhara Venkata Raman; 1981 Nobel Prize winner in Physics Kai Siegbahn; 2007 Nobel Prize winners in Physics Peter Greenberger and Albert Fert; 2007 Nobel Prize winner in Chemistry Gerhard Eitel; 2010 Nobel Prize winners in Physics Konstantin Novoselov and Andre Geim; 2016 Nobel Prize winners in Physics David Thouless, Duncan Haldane, and Michael Kosterlitz; 2018 Nobel Prize winners in Physics Arthur Ashkin, Gerard Mourou, and Donna Strickland; from [www.nobelprize.org](http://www.nobelprize.org)). Thus, it is no doubt that each innovation in this field generates much profit mainly from the theoretical breakthrough and the subversive novel concepts in basic physics and chemistry, particularly the condensed matter physics and interface chemistry, and the related measurement and characterization technology, besides the invention of the advanced fabrication and synthesis technology. These innovations will enable

*Inorganic and Organic Thin Films: Fundamentals, Fabrication, and Applications*,  
First Edition. Edited by Yujun Song.

© 2021 WILEY-VCH GmbH. Published 2021 by WILEY-VCH GmbH.

the discovery of several singular physical phenomena and materials (e.g. topological semimetals: Dirac semimetal, Weyl semimetal, nodal-line semimetals, and triple degenerate semimetals [3]; one-dimensional van der Waals [4]). Sequentially, these innovations promote the application of the finally constructed devices, equipment, and instruments using thin films and coatings as building blocks extending into novel fields (e.g. 2D transistor [5], extremely huge magnetoresistance [3]), and/or upgrading the conventional fields (e.g. rollable optoelectronic devices, such as flexible and foldable organic light-emitting diode [OLED], and graphene enforced rubber composites for industrials [6–9]). (<https://china.Huanqiu.com/article/9CaKrnJY80x>; <http://en.tireworld.com.cn/cnews/201937/6540.html>; [http://www.gianroitire.cn/gianroitire/vip\\_doc/12760379.html](http://www.gianroitire.cn/gianroitire/vip_doc/12760379.html)). These will lead to the revolution of modern science and technology and then to societal reform toward a high-level civilization. Thus, thin films and coatings have been instrumental in bridging the academic studies and their industrial applications and the society.

Sources, energy, environment, and sustainable development are four fundamental themes of the society that we use to provide the basic necessities of life: food, clothing, shelter, and transportation. These themes depend on the continuous technology innovation in information, transportation, communication, and public health and safety supported by the basic research in physics, chemistry, biology, and life science. Now, several issues and crises arise related to source-, energy-, and ecology-related sustainable development as well as ultrafast and high-throughput communication related to security, public health, national defense and homeland security, etc. Technologies derived from thin films and coatings have been used to develop tools.

## 1.2 Thin Films for the Innovation of Information Technology

In the development of information technology, in order to satisfy the precise navigation for the exploration of outer space and the highly efficient nanosatellites, rapid processing of huge data and long-distance communication are needed, and the related devices should be as small as possible. With the progress of data processing and information technology, this requirement is desired not only in astronautics and aeronautics but also in many other military and society fields, leading to the formation of subversive concepts in miniaturized devices and the planar fabrication technology. Finally, silicon-chip-based thin-film fabrication via photolithography and the subsequent e-beam lithography appears formatting a brand-new industrial field: microelectronics. This requirement also intensively promoted the basic research progress in condensed matter physics (e.g. Si-based semiconductors; complementary metal-oxide semiconductors [CMOS]), chip processing technology for chip-based thin-film devices (e.g. field emission transistor [FET]; vertical transistors [10]; laser emission diodes [LED]), and microelectronic device assembly (e.g. integrated circuit), and various data and imaging processing technologies (e.g. graphics processing unit [GPU] derived software) for information technology. Particularly, several novel physical phenomena or findings related to the surface/interface effects

are discovered in the thin films constructed by multilayers of magnetic, electronic, and optical materials, such as magneto-optical effects, giant magnetoresistance (GMR) effects, colossal magnetoresistance (CMR) effects, and tunneling magnetoresistance (TMR) effects. A more intensive study was carried out to investigate the effects of the new physics of these thin films (see Chapters 1, 2, 5, 9, and 10), which further boosted the fundamental physics progress and simultaneously widened the range of applications of computer science and communication technology in industries. As the related large-scale economical fabrication/processing technology was developed along with the progress and interconnection of the physical technology, chemistry synthesis, and materials science and engineering, these concepts and technologies were realized commercially, thus enabling profit generation by the primarily funded enterprises, which can invest more in basic research and advanced technology, forming a benign circling of this field.

With the information technology development, more application concepts have been advanced (e.g. 3D vision and artificial intelligence [AI] technology), and ultrafast high-throughput data and image processing technology and the related information security are needed. The current Si-based chip information technology can no longer satisfy this demand since the integration limited by the feature size of the Si-based chip will reach the ceiling against Moore's law in the near future. Therefore, more and more novel technical concepts or terms emerge with the rapid technology evolution, such as quantum computer, quantum regulation, quantum information, magnetron light quantum, quantum entanglement communication, and long-distance low-loss optical communication. These concepts have initiated new findings, technologies, and related theoretical studies, such as spintronics, spin-orbital coupling, single photo control, the quantum anomalous hall effect (QAHE), quantum key, room-temperature superconductivity, and high k-space lasing in a dual-wavelength quantum cascade laser technology.

In the literature, thin films have been reported as important media that can be used in technologies that need new materials to be further designed. As a result, many new materials for thin-film devices have been explored, such as two-dimensional (2D) materials (e.g. graphene [Gp]; black phosphorus: P-Hg; hexagonal boron nitride [hBN]; transition metal dichalcogenides [TMDs]:  $\text{WSe}_2$ ,  $\text{MoS}_2$ ), topological insulators (e.g. (Hg, Cd)Te 2D materials [11]  $\text{Bi}_2\text{Se}_3$  nanoribbon [12]), magnetically doped topological insulators enable the QAHE [13], van der Waals heterojunctions (more than one single-atom layer of 2D materials organized using van der Waals force, such as magic-angle graphene [14], TMD/Gp [15], graphene/hBN [16, 17]), nanostructural hybrid multilayered thin films of high magneto-optical effects [18–22], metasurface [23–27] and metastructures [28], etc.

Clearly, the development of large-scale thin-film fabrication methods at low cost is primarily required for high-performance devices fulfilling their industrial applications. Besides the conventional fabrication methods (e.g. physical vapor deposition, ion implanting, chemical vapor deposition [CVD], epitaxial growth, nanoimprinting, mechanical exfoliation from bulk crystals), large-scale high-resolution reliable synthesis and fabrication technology have been developed in the past decades. The fabrication limit has reached sub-10 nm line precision and then atomic resolution

fabrication or even subatomic resolution, particularly in the two-dimensional (2D) materials based thin films [10, 13, 29] or sensing devices based on single molecular assembling thin films [30, 31] or single molecular sensor-assembled thin-film devices. Two-dimensional materials contain electrons that can only move freely in non-nanoscale (1–100 nm) objects, such as nanoscale films, superlattices, and quantum wells. Two-dimensional heterojunctions can combine individual layers of different properties in the atom resolution, which can be used to study and understand the exhibited novel physical phenomena that can be further employed for potential applications. The availability of numerous different 2D materials – with different band structures, from semimetals to semiconductors to insulators – also makes it possible to assemble unique materials with well-designed band alignments [32]. Particularly, 2D materials based on thin films, consisting of 2D heterojunctions/heterostructures formed by atomically thin crystal layers bound by the van der Waals force, have attracted much interest because of their potential in diverse technologies, including electronics, optoelectronics, and catalysis. Therefore, 2D thin films are used as an example to exhibit this prerequisite and their development.

The self-assembly approach to materials synthesis is generally related to the strong chemical bond to hold different components together (e.g. epitaxial growth via biaxially textured technology, molecular beam epitaxial and metal organic CVD), which is usually limited in those materials of highly matched crystal structures and compatible process. Now, this strategy can be extended to the weak van der Waals interaction to pre-assemble the chemical building blocks physically to realize the fabrication without chemical bonds (e.g. van der Waals heterojunctions), which can avoid the limitations of crystal lattices and manufacturing process [33]. Thus, there are two important kinds of 2D heterostructural materials that can be developed conveniently for the fabrication of microstructures for more tunable physico-chemical properties of thin films and coatings. One is the 2D heterostructures stacked by strong bonding (e.g. GaN/NbN epitaxial semiconductor/superconductor heterostructures [34]), and the other is the very popular 2D heterojunctions stacked by van der Waals force (e.g. magic-angle graphene). The function of the 2D heterojunction or heterostructures can be flexibly modified according to the “embedded” design theory. They can be used to assess and reduce the difficulty encountered in the bandgap regulation of a single component [16] and the low on/off current ratio caused by the semimetal nature of single component graphene-based devices [10]. The “embedded” design theory for 2D heterojunction/heterostructures can be conveniently used to fabricate novel highly efficient electronic devices (e.g. vertical transistors formed by graphene/molybdenum ditelluride [MoTe<sub>2</sub>]) [10] and optoelectronic devices [13]. Therefore, the “embedded” design theory for 2D heterojunctions can have fewer components to realize the high-performance analog signal modulation, avoiding the limit of miniaturization with increasing demand on energy in the conventional metal oxide semiconductor field-effect transistor (MOSFET). A wide perspective in the telecommunication field would be developed due to their vast application in the high-performance analog circuits.

There are currently two kinds of methods that have to be developed here for the fabrication of the emerging research field of thin films, such as the 2D

heterojunctions, the topological insulators [35] and the topological semimetals [10]: One type is the top-down physical methods, such as the intercalation/stripping method [36] and the liquid-phase [37] or liquid–air interface assemble [38], usually relating to the progress in physical fabrication. Another type is the “bottom-up” methods, usually relating to chemistry synthesis, such as the gradually modified on-surface synthesis technology. These approaches may require the conventional epitaxial growth (e.g. molecular beam epitaxy [MBE]) process [34] or doping steps [13] to prepare some of the 2D layers. Of course, the first prerequisite for the two types of fabrication methods is the 2D materials, many of which have to use chemistry methods firstly.

Among 2D materials, the 2D semiconductors, such as  $\text{MoS}_2$  or  $\text{WSe}_2$ , have great applications in the large-scale thin-film electronics. However, the synthesis of high-quality soluble-processing 2D semiconductor nanosheets, nanoribbons, or nanoflakes remains challenging. A general intercalation/stripping approach was recently developed by Duan and Huang group [36] for the preparation of highly uniform, solution-processable, phase-pure semiconducting nanosheets. This process involves the electrochemical intercalation of quaternary ammonium molecules (such as tetraheptylammonium bromide) into 2D crystals, followed by a mild sonication and exfoliation process. Phase-pure, semiconducting 2H- $\text{MoS}_2$  nanosheets with a narrow thickness distribution can be obtained, which can be further processed into high-performance thin-film transistors. The structure and composition of the exfoliated  $\text{MoS}_2$  nanosheets obtained was characterized by this approach [36]. The scalable fabrication of large-area arrays of thin film transistors can be further fabricated, enabling the construction of functional logic gates and computational circuits, including inverter gates, NAND (neither agree nor disagree [surveys]) gates, NOR gate, AND (agree nor disagree) gates, and XOR (exclusive-OR) gates, and a logic half-adder [36]. This kind of solution-processable method can be extended to fabricate many other high-quality 2D nanosheets for large-scale electronics, such as  $\text{WSe}_2$ ,  $\text{Bi}_2\text{Se}_3$ ,  $\text{NbSe}_2$ ,  $\text{In}_2\text{Se}_3$ ,  $\text{Sb}_2\text{Te}_3$ , and black phosphorus.

In addition, even the traditional method can be further developed into sophisticated technologies by combining them with some advanced instruments in thin-film fabrication. For example, the “tear and stack” technique for graphene fabrication [39] can be further developed by combination with layer exfoliation, electron-beam lithography, and reactive ion etching (RIE) to a modified “tear and stack” technique for the precise angle control in the fabrication of the stacking 2D superlattices [14]. The success of this method has made it possible to synthesize two different layers with controlled stacking angles, such as the magic-angle graphene superlattices, which provide the essential materials to study their correlated insulator behavior at half-filling in magic-angle graphene superlattices for exotic quantum phenomena [14] and to reveal their unconventional superconductivity [35].

Even though the epitaxial growth (particularly molecular beam epitaxial growth) approach is still the main “bottom-up” technology for the 2D films including semiconductors and their heterojunction and van der Waals heterojunctions [34], a new bottom-up method, or the on-surface synthesis technology, has been gradually

developed for large-scale synthesis of 2D heterojunction thin films at atomic precision (e.g. heterostructural nanoribbon assembled thin films) [29, 40]. This method entails using the precursors to synthesize ribbons with controlled width and edge microstructures on the oriented crystal surfaces of the metal substrates. The basic fabrication steps of the on-surface synthesis process using graphene nanoribbons (GNRs) as models to produce the prototypical armchair graphene ribbon of width  $N=7$  obtained using 10,10'-dibromo-9,9'-bianthryl as precursor are schemed [40]. The metal surfaces are usually very clean Au(111) and Ag(111) single crystals as well as 200 nm Au(111) thin films that are epitaxially grown on mica for GNR growth. Thermal sublimation of the monomers onto a solid substrate surface is firstly conducted to remove their halogen substituents, yielding the molecular building blocks of the targeted graphene ribbon in the form of surface-stabilized biradical species. During the first thermal activation step, the biradical species diffuse across the surface and undergo radical addition reactions to form linear polymer chains as imprinted by the specific chemical functionality pattern of the monomers. Then, a surface-assisted cyclodehydrogenation is performed in the second thermal activation step establishing an extended fully aromatic system. For the fabrication of straight  $N=7$  armchair GNRs, the substrate is maintained at 200 °C during monomer deposition to induce dehalogenation and radical addition. After deposition, the sample is post-annealed at 400 °C for 10 minutes to cyclodehydrogenate the polymers and form GNRs. For the chevron-type GNRs, the preparation is identical using another precursor monomer 2: 6,11-dibromo-1,2,3,4-tetraphenyltriphenylene monomer, except for the fact that slightly higher substrate temperatures of 250 and 440 °C are used during monomer 2 deposition and for post-annealing, respectively. In both cases, essentially all deposited monomers are attached to the GNRs, spontaneously transforming into the desired GNR structures. This approach is versatile for the on-surface synthesis of GNRs of different widths and edges, controlled by the monomers and reaction conditions.

Ultrasmall transistors – and thus the next step in the further miniaturization of electronic circuits – are the obvious application possibilities. Although they are technically challenging, electronics based on nano-transistors actually work fundamentally the same as today's microelectronics. The Empa researchers would produce transistors with a channel cross section 1000 times smaller than those typically manufactured today from semiconducting nanoribbons. However, further possibilities are also feasible, for example, in the fields of spintronics or quantum informatics [41]. These nanoribbons can self-assemble to dense monolayered thin films via the well-established self-assembly for the further precise study of their microstructure dependent properties that some of them may be only theoretically studied years ago. Thus the on-surface synthesis technology makes it possible to fabricate the nanostructured thin films at the atomic resolution to realize the experimental study for some theoretically predicted physical effects or phenomena in atomic-scale thin films. The typical examples can refer to the different origins of energy gaps for GNRs with armchair-shaped edges and with zig-zag-shaped edges calculated by *ab initio* calculations according to the first-principles approach [42], and the existence of symmetry-protected topological phases, junction states, and

spin centers in armchair-edge graphene ribbon systems, and the interesting topological phases protected by the spatial symmetries in the chevron GNRs and cove edged GNRs [43]. The topological nontrivial and trivial study of GNRs [29] can be further extended due to the success in the precise synthesis of the graphene nanoribbons of different edge structures and controlled widths (e.g. zig-zag, armchair). Steven G. Louie advanced the armchair topological band engineering of GNRs, which classify them as topological nontrivial and topological trivial according to the difference in the width and the edge microstructure [29]. As the two GNRs of different types (e.g. nontrivial and trivial) are intersected, the interface state of topology protection (the zero-energy state) will be formed. The GNR with armchair edge preserves the width-dependent semiconducting properties, and that with zig-zag edge preserves the magnetic side. The simulated result suggests that the edge state at the same side has the same spin states and preserves the ferromagnetic property, while the spin state of the other edge state is contrary to this edge, leading to the antiferromagnetic property in the whole ribbon [42].

Besides the abovementioned progress in the fabrication of the 2D heterojunctions or heterojunctions, the liquid–air self-assemble process has been developed by Christopher B. Murray group 10 years ago [38]. The liquid–air self-assemble approach can be treated as a cost-efficient and convenient approach by arranging varieties of monodisperse nanomaterials to form heterogeneous thin films by adjusting the interface interaction between the nanomaterial solution and the air. This method straightly expanded the precision of the nanosphere Lithographie, Galvanoformung, Abformung (LIGA) process [44, 45] from several hundred nanometers to 10 nm or higher. Clearly, this approach significantly depends on the synthesis of monodisperse nanoparticles (NPs) and the matched interface between the liquid solution and air, which can possibly reach sub-10 nm resolution to assemble different nanoparticles to varieties of heterogeneous nanoparticle arrayed thin films.

### 1.3 Thin Films for Ultrasensitive Sensing Devices

One of the main goals to develop large-scale thin-film fabrication methods and study their structure–property relationship is to manufacture ultrasensitive sensing devices. Besides the integrated circuit design and manufacture process for their application in high-performance computers, the assembling and integrating methods (e.g. microelectronic mechanics [MEMs] approach) are needed to realize their application in other fields, which can process thin films into active devices and couple with necessary outer instruments (e.g. display, data processing devices) even though “interfaces themselves are devices.” With the progress of thin-film fabrication, processing thin-film based devices into ultrasensitive sensors have evolved from the traditional MEMs to the advanced nanoelectronic mechanics (NEMs) and then to atom-scale electronic mechanics (AEMs) or single molecule electronic mechanics (details can be referred to Chapter 6). In addition, the continuously developing template-assisted nanoimprinting methods, template transfer nanoimprinting molding process [18, 20, 22, 46–49], can be conveniently

coupled with other advanced nanoimprinting approaches (e.g. e-beam LIGA, super-resolution lithography) due to their flexibility in some special nanostructure (e.g. nanopore, nanolace) fabrication at large area economically, which can be used in the sensing film fabrication economically for MEMs, NEMs, and AEMs for ultrasensitive electronics, optoelectronics, magnetic detectors, and other kinds of flexible sensors.

One of the important applications in thin films is the flat screen for video information display. OLED are still the fastest growing technology in the display industry even though only one chapter in this book discusses one topic related to this field in this book (referring to Chapter 11) [50]. OLED is an emerging display technology that enables beautiful and efficient displays and lighting panels. OLEDs are already being used in many mobile devices and TVs, and the next generation of these panels will be flexible and bendable. One of the many benefits of OLEDs includes its manufacturability on rigid (glass) or flexible substrates. A number of technologies are required for the fabrication of OLEDs on flexible substrates or foldable OLEDs (FOLEDs). FOLEDs are OLEDs built on nonrigid substrates such as plastic or metal foil. This enhances the durability and enables conformation to certain shapes and even repeated bending, rolling, or flexing. FOLEDs, still in their infancy, will usher in a range of new design possibilities for the display and lighting industries. Imagine having a mobile phone that looks like a pen but has a bright, full-color display that rolls in and out for use, which is called the Universal Communication Device™ (UCD). In the future, it may be very common to open a foldable smartphone from your pocket into a tablet display, to roll up a television into your pocket, and to use conformable transparent interior lighting panels that could be unbreakable. These ideas offer, you should believe, a mere glimpse into the wonders and possibilities that FOLEDs offer. The market can reach US\$ 63 billion in 2030 predicted by IDTechEx company (<https://www.idtechex.com/en/research-report/flexible-printed-oled-displays-2020-2030-forecasts-markets-technologies/693>).

Simultaneously, the flexible and wearable devices [51] have also been developed rapidly together with the progress of flexible OLED technology [50, 52, 53], providing much convenience in dreaming light and acoustic tasting of new technology making new life. If we can fabricate these abovementioned 2D materials under the progress of these thin-film fabrication and device assemble technology, the invention of ultra-thin flexible and foldable sensing devices and more efficient OLED displays will be of interest.

In addition, thin films are always associated with nanotechnology and precise atom manipulation based on interface physics and chemistry. Introducing nanostructures or atomic structures into thin films can even sprout an old academic field. For example, nanoporous magnetoplasmonic thin films developed by Song's group can enhance the amplitude of the Fabry–Perrot interference and tune their optical oscillating into infrared (IR) range with wavelength at least from optical range to 2600 nm due to the surface plasmon resonance-enhanced Fabry–Perrot interference in the nanoporous structures [18, 47]. They also discovered the optical cavity-enhanced magneto-optical Kerr effect with a distinct reversed magneto-optical Kerr signal [22] and further improve the Raman scattering signals

for biosensors by careful design of pore size, depth, interspacing, and components of the multilayered nanoporous thin films [54].

Acousto-optical devices, such as modulators, filters, or deflectors, implement a simple and effective way of light modulation and signal processing techniques. However, their operation wavelengths are restricted to visible and near-infrared (NIR) frequency region due to a quadratic decrease of the efficiency of acousto-optical interaction with the wavelength increase. At the same time, almost all materials with a high value of acousto-optical figure of merit are nontransparent at wavelengths larger than  $5\ \mu\text{m}$ , while the transparent materials possess significantly lower acousto-optical figure of merit. Daria O. Ignatyeva's group designed a hybrid nanostructural Otto structural thin film to overcome this limit [21]. Their results indicated that the acousto-optical light can be modulated to the mid-infrared spectral range (more than  $5\ \mu\text{m}$ ) by the planar semiconductor structures supporting guided modes at low loss using this kind of Otto-type multilayered nanostructures (i.e. semiconductor prism/noble metal/acoustic piezoelectric). Belotelov et al. also demonstrated that magnetic field sensors based on magnetoplasmonic effects can be theoretically up to a detecting resolution of  $\text{fT}/\text{Hz}^{-1/2}$  if designing nanostructural thin films with a high-quality  $Q$  factor [19]. We can expect that the detecting resolution for a weak magnetic field can be further increased, possibly up to  $\text{aT}/\text{Hz}^{-1/2}$  if other physics fields (Fabry–Perrot interference, electric field, localized surface plasmon resonance induced near field) or effects (inversed Hall effect, spin-orbital coupling effect), can be coupled into the magneto-optical effects. Clearly, success of these devices is the result of the strength to leverage multiphysics coupling by designing suitable multilayered nanostructural thin films. In the future, the combination of nanotechnology with the multiphysics coupling may address many other limitations in the ultrasensitive sensor development by precisely constructing suitable nanostructured thin films.

## 1.4 Thin Films for Sustainable Energy Application

The rapid development of human society enforces consumption of more and more energy and resources. It is difficult for our current science and technology to achieve zero pollution and perfect recycling, leading to eco-environment deterioration. Now, people still face resource crisis, energy crisis and ecocrisis. Thin-film technologies have been impinging into these fields to address some issues in these crises. Facing the energy crisis, the sustainable and/or zero pollution energy and the related technology including energy-saving and recovery technology are desired. Solar energy, geothermal energy, and ocean energy are promising sustainable primary energy, and hydrogen energy is one of the real zero-pollution potable energy. These technologies can simultaneously address the eco-crisis because less wastes and environmentally harmful gases will be discharged into our ecosystem.

The escalating energy demand for efficiently running the modern society requires the exploration of clean alternative or sustainable energy and the development of new and effective materials for energy conversion, storage, recovery, and

transfer. In the past decades, new kinds of solar cells based on thin films and coatings (e.g. multilayer heterostructure semiconductor coating cells, thin-film cells, and perovskite coating cells), thermoelectric (TE) thin films, and the related proton-exchange membranes (PEMs) for hydrogen fuel cells (FCs) have been developed intensively. In addition, lots of 2D materials (e.g. graphene) have been used in the fabrication of high-performance film-based electrodes for new batteries, such as the scaffold or interfacial layer for lithium-metal anodes and the cathode for Li/Na–O<sub>2</sub> batteries in the past decades [55].

The thermoelectric (TE) process is fundamentally a microscopic one involving the transport and exchange of energy by and between electrons and lattice vibrations or phonons, in a solid (i.e. TE materials). The TE process is generally based on the oldest basic thermoelectric phenomena of the Peltier and Seebeck effects [56, 57]. TE generators are fabricated based on the Seebeck effect or an electrical potential being generated when there is a temperature difference across a piece of TE materials (e.g. Bi<sub>2</sub>Te<sub>3</sub> [58], PbTe [59], and SiGe [60]). Thermoelectric power generation has been significantly pioneered by NASA to overcome the energy issue faced by some special missions, such as the interstellar mission of Voyager-1 launched in 1977. Solar cells and other energy sources are infeasible in this kind of interstellar mission because of the extended distance from the sun or operating on densely shielded planets. Thus, the radioisotope thermoelectric power generator (RTG) was invented, by which the heat generated by the radioactive decay of a <sup>238</sup>Pu source can be converted to the electrical power by a thermoelectric generator (<http://voyager.jpl.nasa.gov/index.html>). Since then, many other NASA missions have been powered by RTGs. The most famous example is the Mars Science Laboratory, “Curiosity” rover (<http://mars.nasa.gov/msl>).

Thermoelectric generators have been currently much actively being pursued and used as the main power supply by the National Aeronautics and Space Administration of many countries in the aeronautic project and the astronautics exploration. Due to the capability of directly converting heat into electricity by the utilization of small temperature difference, TE materials have also shown great potential to generate electricity particularly from the industrial waste heat, geothermal source, ocean thermal gradient, and body thermal in the past decades. These heat sources are previously much difficult to be utilized by traditional energy transfer technology. They are promising materials for power generation from environmentally friendly sources, thus reducing our dependence on fossil fuels and the associated risk of a future energy crisis. Inversely, the Peltier effect can provide all-solid-state heat pumping under electrical activation for climate control, such as Peltier coolers and portable refrigerators. Peltier coolers are often implemented in a charge-coupled device (CCD) detectors or in the heat sinks of microprocessors for reliability and precise temperature control. Due to small size and the absence of moving parts and hence no vibrations, TE niches and thin films can be used to make portable picnic refrigerators and flexible thermal or electric devices in cooling microelectronics (e.g. CPU chips) and optoelectronics (e.g. infrared detectors, laser diodes) [61]. Most microelectronics and optoelectronics devices require responsive small-scale or

localized spot cooling that does not impose a large heat load, which is best satisfied by the thermoelectric refrigeration or coolers [62].

Terrestrial applications of thermoelectric power generation and all-solid-state heat pumpers have become more pertinent. Their unique features of TE materials have led to surging interest in the basic research in TE materials and structure design of high efficiency in the past decade, such as the band structure engineering and the nanoscale effect in the electron crystal and phonon glass [63–67]. The study has promoted the mature of the TE materials design and found lots of novel TE materials, such as varieties of nanocomposites (e.g. lead-antimony-silver-telluride family:  $\text{PbTe-AgSbTe}_2$ ; Pb-chalcogenide nanocomposites),  $\text{PbTe}_{1-x}\text{Se}_x$ ,  $\text{YB}_{66}$ ,  $\text{CeFe}_4\text{Sb}_{12}$ , tetrahedrites ( $\text{Cu}_3\text{SbSe}_4$ ),  $\text{MgSb}_2$ , La, and Fe- or Co-doped Ca–Co–O misfit-layered cobaltites, and filled skutterudite antimonides [67–70]. Recent progress in new thermoelectric materials has paved the thin-film power generators of TE materials, which can be referred to in Chapter 8 of this book for details. Up to now, TE applications cover a wide spectrum of heat sources, from utilizing environmentally friendly heat sources to generate electricity, to using body heat for portable electronics, and to using thin-film cooler/generator. The stringent requirements on the Seebeck coefficient, electrical conductivity, and thermal conductivity that are necessary to produce good thermoelectric behavior continue to offer challenges and inspiration to myriad researchers. Thermoelectricity has become a proving ground for numerous new and innovative concepts in physics, chemistry, and materials science, including quantum size effects, nanostructuring, phonon-glass–electron crystal behavior, and large anharmonicity. New knowledge uncovered in these and other areas is driving improvements in material performance, and the future holds the promise that highly efficient thermoelectric devices for both power generation from waste heat and solid-state climate control will become a reality [71]. Given the progress in the understanding of TE, we still want to mention that no single technology can meet the world’s energy needs in the twenty-first century. One needs a combination of many technologies and novel materials into thin films, such as the solar-thermoelectric hybrid power generator of full band range by using TE materials and semiconductors together [72].

Solar energy may be the most popular sustainable clean energy on the Earth. Photovoltaic (PV) technology, such as solar cells harvesting solar energy directly into electricity, has been developed rapidly in the past decades. Besides the semiconductor multilayered thin-film solar cells, the perovskite thin-film solar cells are another viable competitor to the commercially available silicon-based solar cells. Apart from low-cost, simple device processing and manufacturability combined compatibility with roll-to-roll processing and fabrication on flexible substrates add to the merits of the perovskite PV technology by comparing with III–V semiconductor [73–79]. The term “perovskite” was attributed to the crystal structure of calcium titanate ( $\text{CaTiO}_3$ ), which was discovered by the German mineralogist Gustav Rose in 1839 and named in honor of the Russian mineralogist Lev Perovski [80]. The perovskite solar cells (PSCs) present numerous advantages include unique electronic structure, bandgap tunability, superior charge transport properties, facile processing, and low cost [73, 79]. PSCs have demonstrated unprecedented progress in efficiency and its

architecture evolved over the period of the last decade since 2009, leading to the advent of new low-cost PV technology. They can be easily fabricated on the flexible substrates (conductive polymers) by the traditional ink-coating technology and conveniently coupled with other technologies and materials (e.g. graphene, semiconductors, ferroelectrics, Si chip) for enhanced performance. Their power conversion efficiency (PCE) has achieved a high PCE of about 22% in 2016 [79], serving as a promising candidate with the potential to replace the existing commercial PV technologies. This breakthrough led to the so-called “perovskite fever” [81], attracting much research interest in the following years, eventually increasing the efficiency to a record 22.1% (National Renewable Energy Laboratory [NREL]) in early 2016 [79].

PV technology is a multidisciplinary and versatile field in which lots of novel advanced technologies can be coupled with varieties of the related targeting materials, the progress of fundamental research, and even the traditional technologies very well, finding their own strong points and/or creating novel pinpoints to address the issues in solar cells. Much more advanced design methods (e.g. tandem solar cells [TSCs], multi-junction cells such as that formed by semiconductors and perovskites) and fabrication technologies have been invented for the development of more and more types of perovskites (e.g. metal halide perovskite, perovskite-copper indium gallium selenide [CIGS]) of high photoelectric effects after 2016.

In March 2018, Jinsong Huang group [82] developed a molecular (i.e. 2,3,5,6-tetrafluoro-7,7,8,8-tetracyanoquino dimethane: F4TCNQ) additive-assisted strategy for p-type molecular doping of solution-bladed perovskite films (i.e. methylammonium lead iodide: MAPbI<sub>3</sub>) to address the issue of the mismatched energy band between the indium tin oxide (ITO) and the perovskite (Figure 1.1a). Their final fabricated F4TCNQ-doped films exhibiting increased electrical conductivity, especially at grain boundary regions, and increased charge carrier concentrations (Figure 1.1b-j). Molecular doping of perovskite film by F4TCNQ led to the considerable enhancement of PV performance from 11.0% to 20.2% [82]. The simple but effective approach enabled the scalable fabrication of HTL-free PSC devices with a simplified device geometry using the convenient and economical Doctor blading and doping fabrication technique (Figure 1.1).

As one emerging PV technology rooted from the Earth-rich element compounds and the economical and simple solution casting fabrication techniques, PSCs are expected to realize the economic electricity generation. It plays one of the main roles to settle the energy crisis and the ecological deterioration once and for all by fully utilizing solar energy. However, their stability and large-scale fabrication are two obstacles to commercialization. In September 2018, Hongwei Han's and Edward H. Sargent's group summarized the progress of PSCs again and pinpointed the challenges for their commercializing [83]. The power transfer efficiency and stability have been gradually increased after developing various device configurations (including mesoscopic, planar, triple mesoscopic, and tandem structures) and lots of highly efficient materials systems in the past few years [83]. The highest laboratory photoelectric conversion efficiency of PSCs notarized by a third party reached 23.3% in Sept. 2018, which has exceeded the commercial polycrystalline silicon solar cells, the CdTe and CIGS thin-film solar cells, exhibiting the commercialization

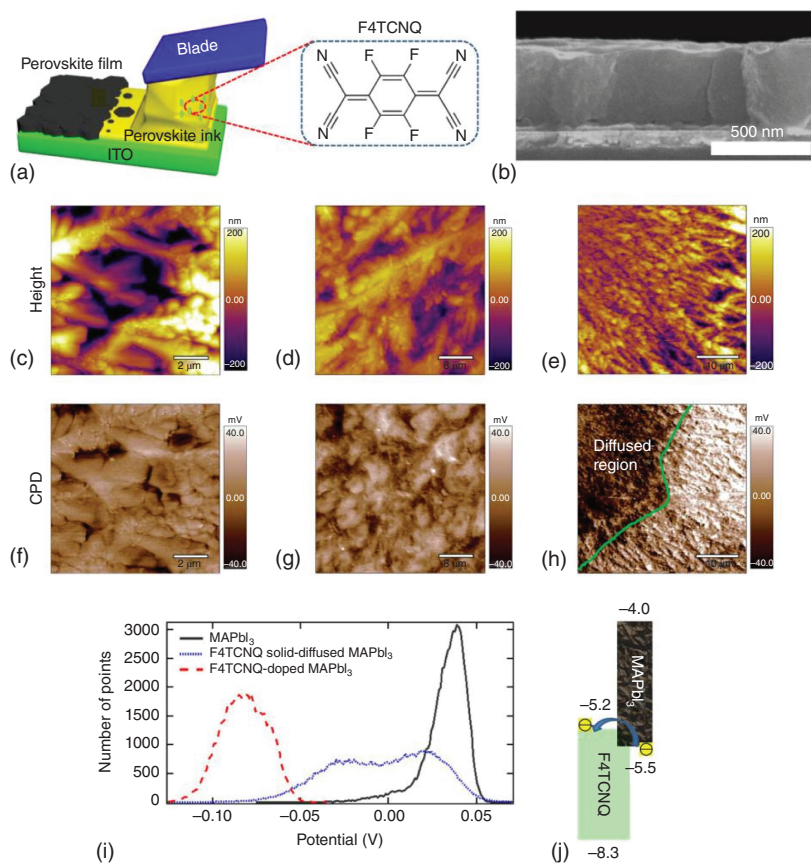


**Figure 1.1** Doctor blading and doping of perovskite films by F4TCNQ. (a) Schematic illustration of a doctor-bladed perovskite film and the chemical structure of the F4TCNQ dopant. (b) Cross-sectional SEM image of the  $\text{MAPbI}_3$  film deposited directly onto ITO glass via bladed coating at  $150^\circ\text{C}$ , showing the film thickness of around 500 nm. Topography KPFM images of (c, f)  $\text{MAPbI}_3$ , (d, g) F4TCNQ-doped  $\text{MAPbI}_3$ , and (e, h) F4TCNQ solid-diffused  $\text{MAPbI}_3$  films. CPD represents the contact potential difference between the tip and the sample's surface. (i) Surface potential profiles of different perovskite films as indicated. (j) Schematic illustration of the energy diagram and electron transfer process for  $\text{MAPbI}_3$ :F4TCNQ blends. F4TCNQ: 2,3,5,6-tetrafluoro-7,7,8,8-tetracyanoquino dimethane;  $\text{MAPbI}_3$ : methylammonium lead iodide; ITO: indium tin oxide. Source: Wu et al. [82]. © 2018, Springer Nature Limited.

perspective and great potential market value. As for the stability of devices, there are varieties of PSCs showing no distinct efficiency damping after the 10 000 hours' standard testing under the required testing conditions (e.g. high temperature, continuous illumination, high humidity) using the simulated sunlight. A  $110\text{ m}^2$  perovskite PV system with printable triple mesoscopic PSC modules ( $3600\text{ cm}^2$  for each) has been launched by Wonder Solar in China.

According to their configurations and coating components for light harvesting, these solar cells can be classified as single-junction GaAs cells, multi-junction cells

(two-terminal, monolithic), crystalline silicon cells, thin-film PVs technologies, and emerging PVs as reported from the National Center for Photovoltaics (NCPV) at NREL of the USA (<https://www.nrel.gov/pv/cell-efficiency.html>). In addition, there are two key top layers in the multi-junction cells: III–V semiconductor top coatings and perovskite top coatings. Particularly, the marriage to other advanced materials (e.g. 2D materials) and the optimized structure design theory have greatly improved the solar energy transfer efficiency and long lifetime after hastening varieties of thin-film solar cells, such as the double-junction (noncondensing) thin-film solar cells and perovskite–silicon stack cells, perovskite-based TSCs, and organic–inorganic solar cells [73, 74, 79].

After three years' accumulation in the theoretical and experimental study and the application transformation since 2016, the PV technology experienced a blowout development after 2019 that is indeed a great year for solar cells. There are so many achievements that deserve our consideration, which can encourage us to have more interest in this vivid field. Some of them will be briefly described as following. Wei Huang group highlighted the current status and recent advances in perovskite-based TSCs, including perovskite–silicon, perovskite–perovskite, and perovskite–CIGS integrations. Figure 1.2 describes the solar efficiency growth of the three kinds of perovskite-based solar cells in the past 4 years [73], among which the perovskite–silicon can reach up to 27.1% near to the theoretical limit or the Shockley–Queisser limit of 33.16%.

Thereby, more attention has to be paid to TSCs that are suggested as an alternative to beat the efficiency limit since a maximum efficiency of 42% can be reached if using two subcells with bandgaps of 1.9 eV/1.0 eV, opening up a great potential to

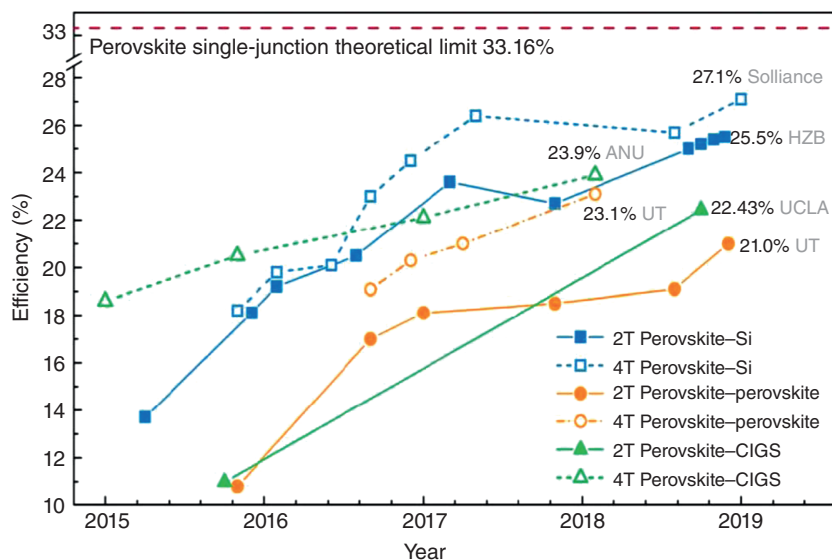


**Figure 1.2** Progress in the efficiency of the perovskite single-junction solar cells in the past five years. CIGS: copper indium gallium selenide. Source: Hu et al. [73].

develop perovskite-based TSCs for commercialization [73]. This kind of TSCs can serve as a promising candidate with the potential to replace the existing commercial PV technologies in the near future [73], as shown in the progress in the early of the following year (2020) (<https://www.nrel.gov/pv/cell-efficiency.html>).

Dion Jacobson (DJ) two-dimensional halide perovskites have been attracting much attention. However, the barrier thickness of the related quantum well (QW) is not well-known even though it is key in the design of highly efficient DJ PSCs. Wei Huang and Yonghua Chen's group designed the efficient DJ thickness by regulating the orientation and uniform dispersion of DJ perovskites via the chain length of large-volume organic ammonium spacers [84]. It was found that the DJ perovskite could have the suitable QW barrier thickness, excellent orientation, and more uniformly dispersed QW if using 1,3-propanediamine (PDA) and 1,4-butanediamine (BDA), leading to smooth bandgap transition, longer carrier diffusion length, higher charger mobility, and lower defect density [84]. Finally, they successfully fabricated DJ-type PV cells with efficiency up to 16.38% using BDA [84].

It is a substantial challenge to prevent the degradation of metal PSCs by humid air to improve their stability and lifetime for their future commercialization. Michael Grätzel's group invented an intercalation method to improve their stability in humid air by forming the 3D/2D bilayer perovskite. This method entails introducing a 2D  $A_2PbI_4$  perovskite layer by employing pentafluorophenylethyl ammonium (FEA) as a fluoroarene cation inserted between the three-dimensional (3D) light-harvesting perovskite film and the hole-transporting material (HTM) [85]. The perfluorinated benzene moiety confers an ultrahydrophobic character to the spacer layer, protecting the perovskite light-harvesting material from ambient moisture and reducing the mitigating ionic diffusion in the device. The 2D layer simultaneously enhances interfacial hole extraction to suppress nonradiative carrier recombination, enabling a PCE up to 22.09%. Surprisingly, their unsealed 3D/2D PSCs can retain 90% of their efficiency during PV operation for 1000 hours in humid air under simulated sunlight.

Rosei and coworkers [86] reported the integrated effects of carbon quantum dots (C-dots) in the fabrication of high-efficiency inverted plane heterojunctions (PHJ) PSCs by using C-dots to modify the hole-transporting layer in the plane PSCs. The PSC efficiency can be up to 16.2% as introducing C-dots onto oxide graphene layers as the hole-transporting layer, whose efficiency can reach 16.8% under the UV range if using C-dots as the downshift layer. The introduction of C-dots can also extract the hole and transfer it to the conductive substrate and delay the charge recombination, leading to the enhanced stability of PSCs.

Energy loss in the hybrid lead halide perovskite cells is interrelated with the non-radiation combination in the interface and the perovskite layer. Liao and coworkers [87] developed a simple but efficient strategy to reduce this loss via the coupling of the external electric field with the intrinsic doping of ferroelectric polymer as the interface polar layer. This strategy entails doping a series of polar ferroelectric (PFE) polymers into the methylammonium lead iodide ( $MAPbI_3$ ) layer and/or inserting them between the perovskite and the hole-transporting layers to modify and/or enhance the build-in field (BIF), improve the crystallization

of MAPbI<sub>3</sub>, and regulate the non-radiative recombination in PSCs. Doped PFE polymers can enable MA<sup>+</sup> orderly arranged to reduce trap states and optimize the oriented growth of the perovskite layer. At the same time, inserting PFE into the gap between the perovskite layer and the hole-transporting layer can enhance the BIF via the widened depletion region in the cell. The consequently assembled cells exhibit an open-circuit voltage of 1.14 V and a PCE of 21.38% [87].

Cost is always one main issue for the commercialization of PSCs. For reducing the materials cost, Mohammad Khaja Nazeeruddin's group [88] developed the synthesis of three enamine HTMs based on TrögerQs base scaffold. The best performing material of HTM3 demonstrated 18.62% PCE in PSCs and presented a markedly superior long-term stability in nonencapsulated devices [88]. Moreover, the high glass-transition temperature (176 °C) of HTM3 also suggests promising perspectives in high-temperature device applications of PSCs.

An organic solar cell (OSC) is another promising PV device, particularly for the flexible portable power providers. Ternary OSCs also show great potential to enhance the PV property of single-junction OSCs. Liu et al. [89] have prepared a series of ternary OSCs using the previously developed PM7: ITC-2Cl [89–91] as the main system, the ultralow-bandgap receptor of IXIC-4Cl as the ternary component. The active absorbance layer can be up to 1000 nm and the PCE of 15.37% with only 0.42 eV energy loss [89].

It is an efficient method to improve the power transfer efficiency for OSCs by intensifying the light absorbance through enhancing the intramolecular push–pull effect of PV materials. However, as for the electron acceptors, the design strategy for halide molecular usually decreases the molecule energy level, leading to the reduced open-circuit voltage. Yao et al. [92] designed and synthesized a kind of chloride non-fullerene acceptor, showing extended optical absorbance and higher voltage than the fluoride compounds. The chloride non-fullerene acceptor can modify the short-circuit photocurrent density and the open-circuit voltage, realizing the PCE of 16.5%. This result indicated that reducing the band gap voltage offset can dramatically improve the power transfer efficiency by precisely tuning the organic PV materials, suggesting the promise of fullerene-free OSCs in practical applications.

The III–V semiconductor solar cells are also one promising type of PV devices because of their high photoelectric efficiency, power density, and stability. However, their expensive manufacturing cost severely impedes their commercialization, partially due to the expensive Ge-based substrates for the epitaxial growth. Oh and coworkers [93] proposed a germanium-on-nothing (GON) technology to fabricate ultrathin Ge films for lightweight and thin GaAs solar cells. As shown in Figure 1.3, the ultrathin epitaxial single crystalline Ge membrane can be formed as the reusable substrate by utilizing the reorganization of cylindrical pores of porous Ge films during hydrogen annealing enable the growth and transfer of GaAs cells. Compared with previous porous Ge studies, the surface quality of reformed Ge can be significantly improved by engineering the initial pore morphology and surface passivation before annealing. The GaAs cells growing on the reformed Ge can have an efficiency of 14.44%, much near to GaAs cells growing on the bulk Ge substrates (16.53%). Their open-circuit voltage is almost the same as those GaAs cells growing

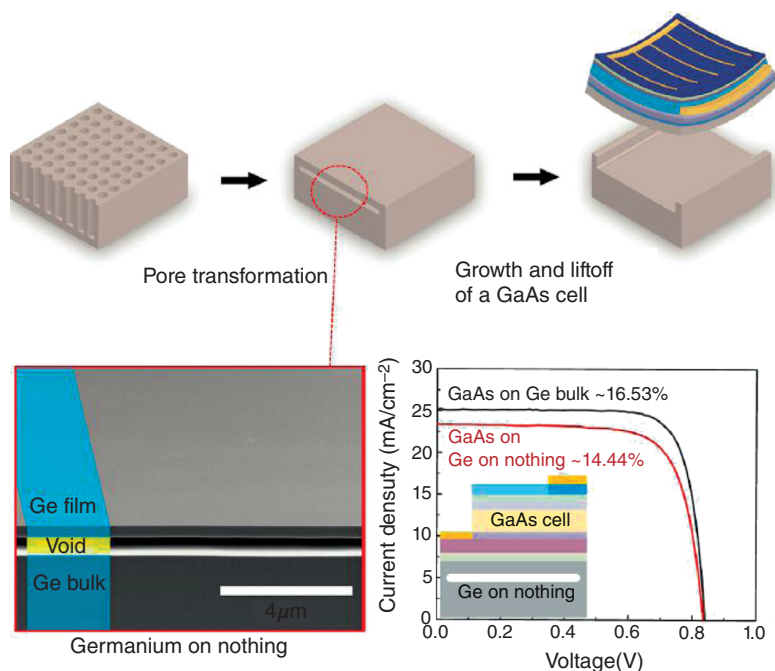


**Figure 1.3** The germanium-on-nothing (GON) technology to fabricate ultrathin Ge films and the GaAs cell, and the voltage-dependent current density curve. Source: Park et al. [93]. Copyright from Elsevier.

on the bulk Ge substrates. This GON technology can reduce the materials cost distinctly of III–V solar cells.

The requirement for flexible electronic and optoelectronic devices provokes the development of flexible energy sources. The flexible composite solar cells have been paid more and more attention recently. With the application of graphene, CVD graphene and the sponge-like 3D reduced graphene oxide (rGO) have been used as a sole HTM in the PSCs, exhibiting excellent performance due to their good deformation features. Cai and Yu in their article on the graphene application summarized this kind of graphene-based flexible PSCs [94]. Figure 1.4 gives the layered structure of this kind of graphene-based flexible PSCs (a,b), V–C curves at different bending radius, and their PCE% and short-circuit currents change with the bending times, showing good cell performance under various bending angles and cycles. These Gp-FPSCs shall have great applications in the flexible folded-potable or wearable electronic and optoelectronic devices [95].

This exciting rapid development of thin-film PSCs continues with the coming of 2020; more and more amazing signs of progress have been achieved. Sargent's group [96] designed  $\text{PbI}_x^{2-x}$  precursor complexes to prepare the metal halide perovskite nanoflakes (PNPLs) with more uniform multi-quantum well distribution based on the idea that iodine-based PNPL permitted wide-band absorbance of sunlight, leading to large Stokes displacement to overcome the bandgap limited absorbance range of the conventional Br based perovskites. Using these I-based nanoflakes,

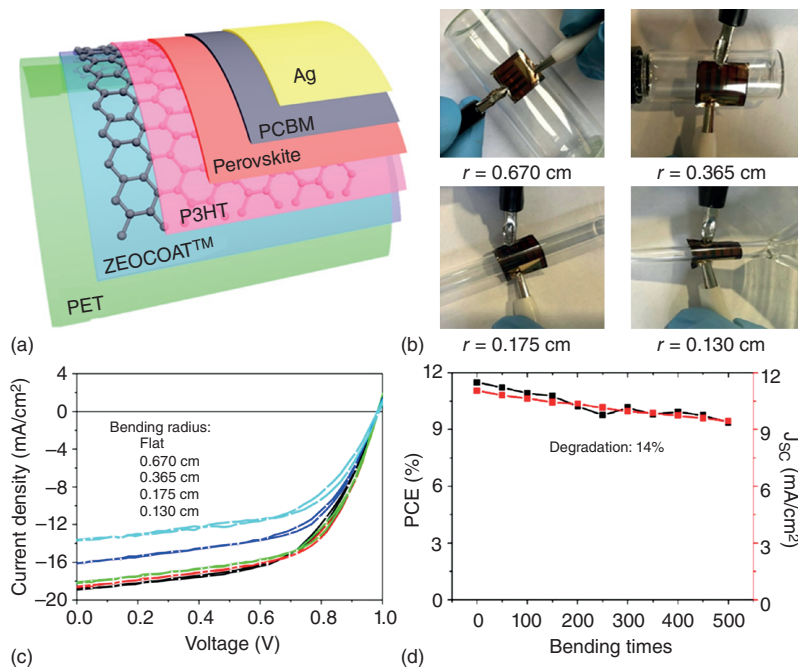


**Figure 1.4** (a) Scheme of layered structures of graphene-based flexible PSCs; (b) pictures of the flexible solar cell units at different bending radius; (c) the C–V curves of the flexible solar cells at different bending radius; (d) the power conversion efficiency (PCE%) change with the bending times (black line) and the short-circuit current (red line). Source: Cai and Yu [94].

they fabricated the luminous solar concentrator (LSC) to realize the highly efficient luminescence. The photoluminescence quantum yield (PLQY) of this kind of thin films can reach up to 56%, and their light scattering efficiency is only 2.0%, which is 1.3 times of the best  $10 \times 10$  cm LSC fabricated under room temperature. Cost is forever one of the key issues for large-scale application of PSCs. Efficient electron transport layer-free perovskite solar cells (ETL-free PSCs) due to their cost-effective and simplified design, high efficiency, and potential compatibility greatly demonstrates the large-area flexible application of PSCs.

However, the absence of ETL usually results in the mismatched interface energy level between the ITO layer and perovskite layer, limiting the charge transfer and collection, which leads to significant energy loss and low device performance [97]. Ge's group invented a method to lower the work function of ITO and optimize the interface energy level alignment by virtue of an inherent dipole by introducing a polar nonconjugated small-molecule modifier to address this issue. The formed barrier-free ITO/perovskite interface is a benefit for the efficient charge transfer and restraining nonradiative recombination, which endows the device with enhanced open-circuit voltage, short-circuit current density, and fill factor. Consequently, the PCE of the modified device can reach 20.55%, much higher than 12.81% of

the ITO-based device, and comparable to state-of-the-art PSCs with an ETL [97]. Moreover, the stability is enhanced with decreased hysteresis effect due to interface defect passivation and inhibited interface charge accumulation. The key advantages of the present device design are the high conversion efficiency potential with simple device structure and the fact that the whole device production process can be carried out at economical and energy-efficient temperatures. This work facilitates the further development of highly efficient, flexible, and recyclable ETL-free PSCs with simplified design and low cost by interface electronic structure engineering through facile electrode modification.

After 60 years of research, the PCE of Si solar cells is approaching the Auger recombination-constrained Shockley–Queisser limit of 29.8% [98, 99]. To further increase the PCE while simultaneously reducing the cost per kWh, new strategies such as tandem configurations have been developed in the past decades. Organometal-halide perovskite/Si TSCs were proposed as one promising candidate to surpass Si efficiency records. A TSC consists of two or more cells that are optically coupled by absorbing different parts of the incident spectrum. This allows for a more efficient conversion of the broad-band solar spectrum into electric power. In a two-cell configuration, the high-energy region of the spectrum is absorbed by the top cell, whereas the transmitted low-energy light is further absorbed by the bottom cell. Hybrid organic–inorganic perovskite-based cells are especially well suited as a top cell for Si-based TSCs due to their high charge carrier mobility, high quantum yield, long diffusion length, sharp absorption edge, and large tunable bandgap covering almost the entire solar spectrum. Several analyses on the limiting efficiency of TSCs have been performed using detailed-balance calculations showing efficiencies up to 69.9% for an infinite number of subcells under 1 sun illumination [100–102].

However, the efficiency of perovskite/Si TSCs is strongly affected by spectral and temperature changes. Consequently, weather conditions at the specific site of deployment should be taken into account when designing perovskite/Si TSCs. Futscher and Ehrler have theoretically suggested in 2016 that perovskite/Si TSCs with PCE limits above 41% are possible for all three tandem configuration even at nonideal climate conditions by using a perovskite top cell with the ideal bandgap for the respective tandem configuration [102]. In addition, it is challenging to monolithically process PSCs directly onto the micrometer-sized texturing on the front surface of record-high-efficiency amorphous/crystalline silicon heterojunction (SC) cells, which limits both high temperature and solution processing of the top cells. The challenge for solar cell design is that both perovskite and Si are finicky. It is well-known that graphene is a 2D material with unique and powerful electronic properties. Graphene is notoriously difficult to work with, and perovskites have a durability issue that needs to be factored into the design. Nevertheless, researchers have been tinkering around with the graphene–perovskite combo to address these issues by utilization of their advantages and suppressing their shortcoming by all in one strategy to fabricate graphene/perovskite/silicon heterojunctions (SCs). To tackle these hurdles, Di Carlo and coworkers developed a mechanically stacked two-terminal perovskite/silicon TSC, with the subcells independently fabricated, optimized, and subsequently coupled by contacting the back electrode of the

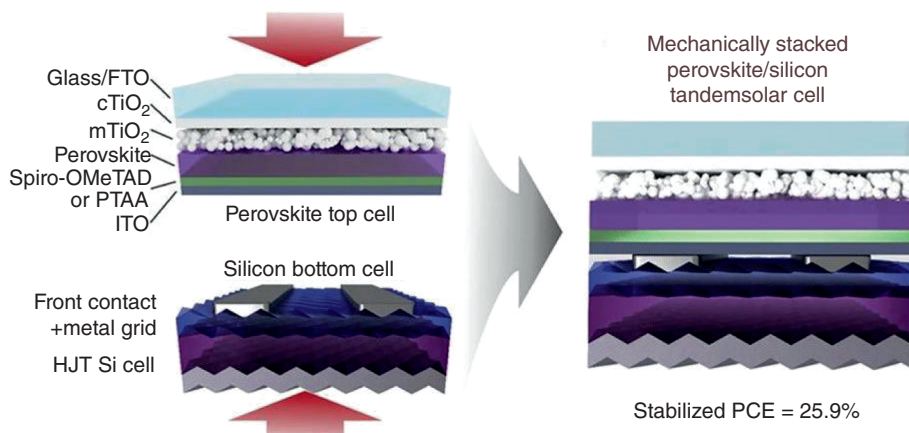


**Figure 1.5** Scheme of the microstructure and the graphene-doped mesoporous electron selective layer mechanically stacked into the perovskite top cell and the silicon bottom solar cell forming the perovskite/graphene/silicon heterojunction tandem SCs. Source: Lamana et al. [103].

mesoscopic perovskite top cell with the texturized and metalized front contact of the silicon bottom cell. The structure and the graphene layer bonding to the heterojunction are schemed in Figure 1.5 [103].

By minimizing optical losses, as achieved by engineering the hole selective layer/rear contact structure, and using a graphene-doped mesoporous electron selective layer (the middle layer between the two layers as shown in the right image of Figure 1.5), the perovskite top cell reaches better electrical performance by graphene doping of the electron selective layer [103]. This heterojunction microstructure design endows a solar cell around those twin challenges and achieved an impressive solar conversion efficiency of 26.3% (25.9% stabilized) over an active area of 1.43 cm<sup>2</sup>, the best solar cell ever of great potential industrialization.

More amazing progress in solar cells is coming in early 2020. On Jan 27, 2020, NREL of the USA announced that the PCE% of single-junction perovskite–silicon stack solar cell invented by Berlin Institute of materials, at Helmholtz (HZB, Germany), has reached 29.15%, exceeding the record of 28% previously reported by Oxford PV company (<https://www.nrel.gov/pv/cell-efficiency.html>). At the same time, groups from Stanford University and Arizona State University declared that the PCE% of their single-junction PSCs was 25.3%, up to the world record kept by Massachusetts Institute of Technology and Korea Institute of Chemical Technology. Finally, and soon, NREL obtained a PCE% of 32.9% in their Double junction (noncondensing) thin-film solar cells. The PCE% of the single-junction perovskite–silicon stack solar cells by HZB was further confirmed and authorized by Fraunhofer Institute of Solar Systems (Germany), updated the record in the PCE% chart of varieties of solar cells (Figure 1.6) by NREL (<https://www.nrel.gov/pv/cell-efficiency.html>); <https://www.nrel.gov/pv/assets/pdfs/best-research-cell-efficiencies.20200128.pdf>; [https://www.helmholtz-berlin.de/pubbin/news\\_seite?nid=21020;sprache=en;seitenid=1](https://www.helmholtz-berlin.de/pubbin/news_seite?nid=21020;sprache=en;seitenid=1)). In this design, a special electrode contact layer

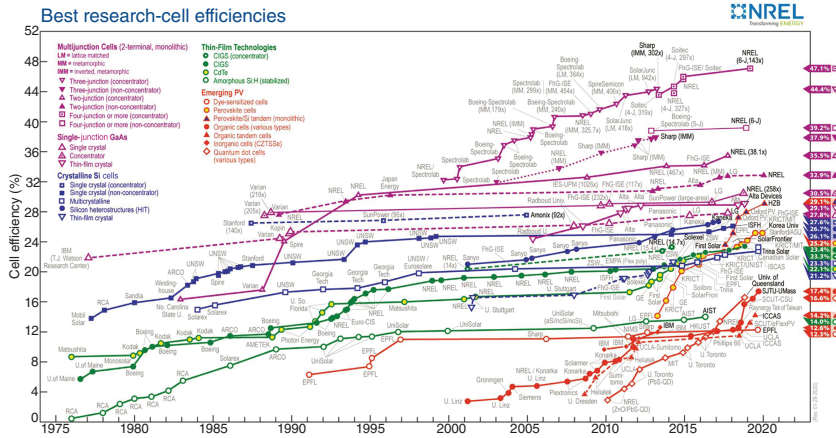


**Figure 1.6** Updated solar cell efficiency by NREL in February 2020 for multi-junction cells, single-junction GaAs cells, crystalline Si cells, cells by thin-film technologies, and cells by emerging photovoltaic technologies. Safe and stable energy storage devices of high energy density at low cost are also essential for our routine transportation and other industrial applications. Varieties of rechargeable supercapacitors and high-performance and high-volume batteries have been developed, such as Li-S batteries, AIBs, and graphene-based supercapacitors [55, 104–107]. The recently developed Li/Na-S batteries and supercapacitors may be the most promising energy storages satisfying these requirements for the next-generation rechargeable energy storage with the rapid coupling of 2D thin-film materials into this field [55, 104]. Metal–sulfur batteries hold practical promise for next-generation batteries because of high energy density and low cost. Development is impeded at present, however, because of unsatisfied discharge capacity and stability in long cycling. Combination of experimental and theoretical approaches can be used to develop insight into the relationship between electrochemical behavior of sulfur redox and metal stripping–plating and the structural properties of electrode materials. With metal–sulfur batteries, two-dimensional (2D) thin-film nanomaterials are a suitable model with which to connect and test experimental results with theoretical predictions and to explore structure–property relationships. Through the view of combining experimental and theoretical approaches, sulfur redox conversion on 2D nanomaterials in various reaction stages was explored, and crucial factors affecting 2D nanomaterials as artificial solid electrolyte interfaces (SEIs) and host materials in protecting Li and Na metal anodes were critically unveiled by Shi-Zhang Qiao [55]. It is indicated that Li/Na-sulfur batteries hold practical promise for next-generation batteries because of high energy density and low cost. Significant progress has been made in understanding mechanisms of sulfur redox and metal stripping/plating with a judicious combination of experimental and theoretical approaches. Two-dimensional (2D) nanomaterials offer a suitable model to correlate experimental results with theoretical predictions and, importantly, with which to explore structure–property relationships. Future research effort should focus on the establishment of correlations between macroscopic conversion kinetics and the electronic structure of the electrode materials with agreed standards and advanced combined experiments and theory. In addition, fabrication of three-dimensional (3D) electrodes from 2D materials might be a promising approach to promote the energy and power densities of the Li/Na-sulfur batteries and other metal–sulfur batteries. Source: <https://www.nrel.gov/pv/cell-efficiency.html>; <https://www.nrel.gov/pv/assets/pdfs/best-research-cell-efficiencies.20200128.pdf>.

was developed for the TSCs, and then, the interface layer was modified. Thus, the top perovskite layer can utilize the optical range of sunlight, and the bottom Si layer of a special  $\text{SiO}_2$  interlayer can transfer most of the IR-NIR light into electric energy, leading to the enhanced PCE% comparing to each single cells.

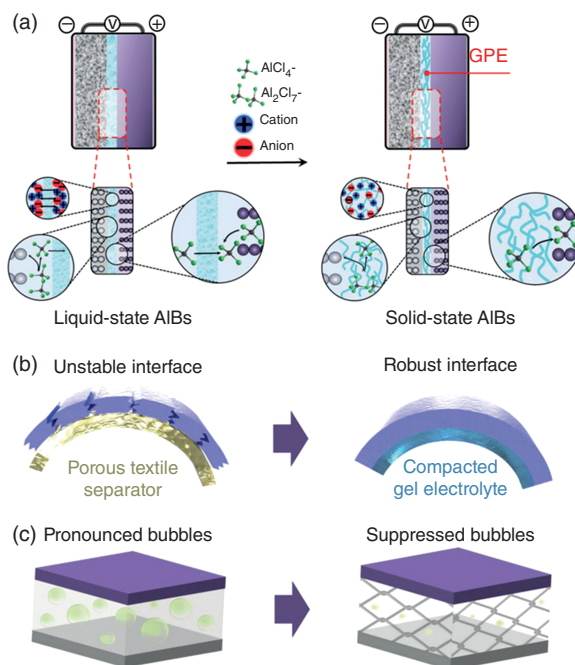
This kind of perovskite/graphene/silicon heterojunction tandem SCs have been fabricated into solar cell modules using the industrial scale fabrication and sealing process for the three kinds of pre-commercialization life testing. They have successfully survived the light resistance test, the damp heat resistance test, and the thermal cycling test on 23 January 2020, which is the first time for the PSCs to realize this goal for commercialization. The PSC modules can be either rigid or flexible and either transparent or semitransparent, which makes them suitable for varieties of application scenarios, such as assembling in windows, roof tiles, external wall faces, roads, sound baffles, and automobile roofs. They can also be colorful via imitation coloring by varieties of structure colors made from the nano/microfabrication. As it is well-known that PSCs and their modules preserve high-efficiency, low-cost processing ability and cheap and rich sources. These marvelous and exciting achievements make PSCs full of perspective for sooner commercialization and serving renewable energy for our routine life.

Rechargeable aluminum-ion batteries (AIBs) are regarded as one promising candidate for post-lithium energy storage systems (ESSs) [107]. For addressing the critical issues in the current liquid AIB systems, here, a flexible solid-state AIB is established using a gel-polymer electrolyte (a kind of electric thin films) for achieving robust electrode–electrolyte interfaces. As shown in Figure 1.7, employment of polymeric electrolytes mainly focuses on addressing the essential problems in the liquid AIBs to transfer into the solid AIBs, including unstable internal interfaces induced by mechanical deformation and production of gases as well as unfavorable separators, which is much different from the utilization of solid-state systems for alleviating the safety issues and enhancing energy density in lithium-ion batteries [107].

Particularly, such gel electrolyte enables the solid-state AIBs to present an ultrafast charge capability within 10 seconds at a current density of 600 mA/g. Meanwhile, an impressive specific capacity  $\approx 120$  mA/h/g is obtained at a current density of 60 mA/g, approaching the theoretical limit of graphite-based AIBs. In addition to the well-retained electrochemical performance below the ice point, the solid-state AIBs also hold great stability and safety under various critical conditions. The results suggest that such a new prototype of solid-state AIBs with robust electrode–electrolyte interfaces promises a novel strategy for fabricating stable and safe flexible ESSs.

Li storage is one key issue for the fabrication of high-performance Li batteries with high volumetric energy density. The carbon allotropes are mainly used as the host materials for reversible lithium uptake in Li-ion batteries [108, 109], thereby laying the foundations for existing and future electrochemical energy storage. Recently, the Li storage in layered 2D materials, such as graphene, has been developed for enhanced Li storage density. However, insight into how lithium is arranged within these hosts is difficult to obtain from a working system because

**Figure 1.7** Overall comparison of liquid-state aluminum-ion batteries (AIBs) and solid-state AIBs: (a) Schemes for the configurations of these two AIBs. (b) Schemes for demonstrating the electrode–electrolyte interfaces: an unstable interface based on porous separator in the liquid-state AIBs and robust interface based on the GPE electrolyte in the solid-state AIBs. (c) Schemes for illustrating the production of gases in the two prototypes of batteries. Source: Yu et al. [107].



the in situ high-resolution transmission electron microscopy (HR-TEM) [110–112] is not suitable to probe those light element, especially lithium (Li) with atomic number less than carbon due to their low scattering cross section for impinging electrons and their susceptibility to knock-on damage [113–115]. This unknown structure–property relation hinders the design and fabrication of more dense Li storage for high-performance Li batteries and the related supercapacitors. Jurgen H. Smet’s and Ute Kaiser’s groups [105] realize the study of the reversible intercalation of lithium into bilayer graphene by in situ low-voltage transmission electron microscopy, using both spherical and chromatic aberration correction to enhance contrast and resolution to the required levels [116]. It is found that lithium atoms can form a multilayered close-packed order between the two carbon sheets [105]. Consequently, the lithium storage capacity associated with this superdense phase far exceeds that expected from the formation of  $\text{LiC}_6$ , which is the densest configuration known under normal conditions for lithium intercalation within bulk graphitic carbon [117]. This finding shall insight the design and fabrication of more dense Li storage for future high-performance Li batteries.

Supercapacitors are another energy storage mode besides the batteries. Thanks to their ultrafast rechargeable ability, high power, long-term lifetime, wide working temperature, and safety, supercapacitors have shown extraordinary promise for potable miniaturized electronics, hybrid electric vehicles, standby power, and field power. However, the power density (i.e. power in unit volume) of the electrochemical supercapacitors is relatively lower than the batteries, which restricts their broader applications, particularly in the potable smart equipment. The power density of supercapacitors needs to be further improved but is usually limited by

electrodes with rather low volumetric performance, which is largely due to the inefficient utilization of pores in charge storage.

Benefited from the progress of the magic materials: graphene and some graphene-based technologies have been invented to address this issue. Recently, a freestanding graphene laminate film electrode with highly efficient pore utilization was developed for the compact capacitive energy storage by precisely tuning the interlayer spacing of graphene laminate films for optimized porosity [118]. The preparation process is as follows [118]: The mixture made from graphene oxide (GO) and thermal expansion reduced graphene (EG) of different ratios were firstly prepared and then vacuum filtrated to form the composite graphene thin film of tunable interlayer spacing, whose layered microstructures are characterized by scanning electronic microscope (SEM). The porosity of the electrode materials can be optimized by regulating the interlayer spacing. By systematically tailoring the pore size matching for the electrolyte ions, utilization of pores and their interspacing can be optimized, and thereby, the volumetric capacitance will be maximized. Consequently, flexible all-solid-state supercapacitors can be fabricated, which can deliver delivers a stack volumetric energy density of 88.1 Wh/l in an ionic liquid electrolyte, representing a critical breakthrough for optimizing the porosity toward compact energy storage [118]. Moreover, the optimized film electrodes exhibit excellent bending ability due to the intrinsic flexibility of graphene [118]. They can further be assembled into ionogel-based, all-solid-state, flexible smart devices with multiple optional outputs and superior stability, demonstrating enormous potential as a portable assembled to smart devices, realizing varieties of output results by designing the suitable circuits [118].

Hierarchically ordered structures with low tortuosity, excellent mechanical flexibility, high optical transparency, and outstanding electrical conductivity are critically important in developing flexible transparent supercapacitor electrodes for innovative applications in electronics and displays. Bionic technology has been recently immersed in the design and fabrication of supercapacitors with the abovementioned microstructures and properties [106]. The leaf-skeleton inspired electrodes have been successfully fabricated by a CVD process, which are reticulated monolithic networks consisting of carbon nanostructures serving as a 3D spongy core and graphene-based films as a protective/conductive shell [106]. The network electrodes show optical transmittance of 85–88%, an electrical sheet resistance of  $\sim 1.8 \Omega/\text{sq}$ , and an areal capacitance of  $7.06 \text{ mF}/\text{cm}^2$  (at  $0.78 \text{ mA}/\text{cm}^2$  in a three-electrode cell) in  $\text{Na}_2\text{SO}_4$  aqueous electrolyte. Flexible transparent and symmetric supercapacitors, based on poly(vinyl alcohol) (PVA)/ $\text{H}_3\text{PO}_4$  gel and the network electrodes, possess a stable working voltage of 1.6 V, energy and power density of  $0.068 \mu\text{Wh}/\text{cm}^2$  and  $47.08 \mu\text{W}/\text{cm}^2$  at an optical transparency of  $\sim 80\%$ , and no capacitance loss over 30 000 flat-bend-release cycles.

Similar to energy storage and utilization of renewable energy source, energy conversion technology is also intimately dependent on thin films and coatings. Energy conversion using electrochemical reactions for fuel cells has attracted increasing attention because of its advantages over traditional fossil energy sources, such as renewability, eco-friendliness, and high efficiency, one of whose key components is

catalytic thin-film based electrodes or catalytic functional PEMs [119, 120]. Among the fuel cell technology, the PEM fuel cells (FCs) may be one of the promising models to determine the factors that influence the commercialization for common transportation, which is based on the highly efficient catalyst filling PEM (i.e. Pt catalyst filling porous Nafion thin films) as the cathodes [121]. PEMs of high electrochemical catalytic performance are particularly desired for the transportation of routine life using zero-waste-releasing potable fuels with high energy density (i.e. hydrogen) if considering the ecological issues as burning fuels of different kinds [122, 123]. Hydrogen fuel cell automobiles have become one popular routine transporter in Japan as Japan has started the FH2R (Fukushima Hydrogen Energy Research Field) model project since 2018, which is just completed at the end of February 2020. The FH2R intends to produce 1200 Nm<sup>3</sup>/hr via a 10 MW water electrolysis system powered by a 20 MW PV device equipped on the 180 000 m<sup>2</sup> field reported from the New Energy and Industrial Technology Development Organization of Japan in March 2020. This model project realizes the perfect coupling between the potable hydrogen fuel cell technology and renewable solar cell technology.

The oxygen reduction reaction (ORR) is a critical factor associated with electrochemical energy conversion in fuel cells. It is an important cathode reaction in many electrochemical energy conversion devices, including hydrogen fuel cells and direct methanol fuel cells [122, 123]. The main difficulty associated with the ORR is the sluggish multiple-electron transfer process, which has to be catalyzed typically by those precious metals such as Pt, Pd, Ru, or their alloys [124–127]. This issue impedes the future common worldwide application. Therefore, the reduction of Pt or precious metal load in the cathode for PEM fuel cells but still keeping high power density is highly needed, particularly reducing the Pt content in the cathode thin films [128–133]. However, the low Pt content in the cathodes will result in the high voltage losses that come from the mass transport resistance of O<sub>2</sub> through the platinum–ionomer interface in the PEM, the location of the Pt particle with respect to the carbon support and the supports' structures. Strasser and Orfanidi group recently proposed a new Pt catalyst/support design that substantially reduces local oxygen-related mass transport resistance [130]. This new design includes the use of chemically modified carbon supports with tailored porosity enabling controlled deposition of Pt nanoparticles on the outer and inner surface of the support particles, resulting in unprecedented uniform coverage of the ionomer over the high-surface-area carbon support thin films, especially under dry operating conditions. Consequently, the present catalyst design exhibits previously unachieved fuel cell power densities in addition to high stability under voltage cycling. Owing to the Coulombic interaction between the ionomer and N groups on the carbon support thin films, homogeneous ionomer distribution and reproducibility during the ink manufacturing process for the catalytic polymer thin films can be ensured.

Another alternative is to develop non-precious catalysts, such as some transition metal (TM) complexes, single-atom catalysts (SACs), or single-site catalysts (SSCs) [121, 134]. TM complexes have been widely used in physical and biological science, particularly playing essential roles in catalysis, chemical synthesis, materials science, photophysics, and bioinorganic chemistry [135–137]. Since 1964, N<sub>4</sub>

macrocycles of non-noble metals (e.g. cobalt) based on the organometallic complexes and bionics have been developed as fuel cell cathode catalysts [138]. Various non-precious earth-abundant metal catalysts, especially those based on transition metal–nitrogen–carbon (MNC) compounds, have been continuously developed to address the issues related to the cost and earth-abundant resources, and their catalytic performance has been gradually enhanced [139–142]. However, these non-precious catalyst-based fuel cells are currently suffering from limited activity, poor stability, poor durability, limited ability for a large-scale yield of high-performance catalysts, impeding their sustainable commercial application by replacing those precious metal catalyst-based fuel cells [128, 143].

Recently, Song's group presents a simple sequenced ultrasonic atomization microreaction, pyrolysis, acid leaching, and calcination process for the mass synthesis of FeNC SSCs with excellent ORR catalytic performance, as shown in Figure 1.8A [121]. The ultrasonic atomization process provides a huge number of microreactors to produce the highly dispersed iron precursors. The subsequent pyrolysis and calcination processes ensure that the iron atoms are conjugated to nitrogen ligands, anchoring them onto carbon black. This synthesis system is eco-friendly by only using water and ethanol as solvents and does not generate pollutant emissions. A combination of various microstructure and composition characterization of these catalysts and the related ORR performance based on these catalysts filling proton-exchange Nafion membrane suggest that the active centers root in the single-atom Fe sites chelating to the fourfold pyridinic N atoms or calling as SSCs. Their electrochemical catalytic ORR performance outperforms the commercial Pt/C catalysts, having much enhanced halfwave potential and kinetic current density (Figure 1.8B) and the substantially enhanced long-term stability and outstanding tolerance to methanol (Figure 1.8B). This synthetic strategy provides a new general method for the eco-friendly large-scale synthesis of high-performance single-atom catalysts for fuel cells.

In addition, even though the large-scale production of hydrogen has recently been realized, the electrocatalysis for water splitting reaction, including hydrogen evolution reaction (HER) and oxygen evolution reaction (OER), is still depending on the catalytic proton-exchange Nafion thin films filled with Pt or other precious-metal-based catalysts. Therefore, similar to those catalysts for the catalytic thin films in ORR, reducing the precious metal loading in catalytic thin films or developing non-precious-metal-based catalysts for HER and OER are desired to further reduce the price of hydrogen as the economic portable fuel [127, 144, 145]. The late strategy is most desired since those precious metals particularly for Pt are nonrecyclable Earth-deficient sources. In particular, for both the OER and HER in electrolysis, it is necessary to develop non-precious, efficient, and durable catalysts. Considering the cost and yield efficiency, it is greatly desired for highly efficient bifunctional catalysts for overall water splitting in an alkaline medium. The transition metal oxides, metal sulfides, metal phosphides, layered bimetallic hydroxide (LDH), and metal alloys have been investigated as the catalysts for OER and HER, whose catalytic performance can be improved through morphology engineering, composite, and doping technology. Particularly, FeNi alloy and their

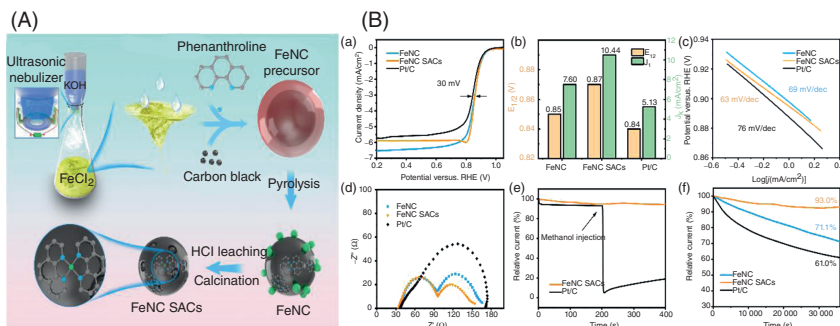


**Figure 1.8** (A) Schematic of the preparation of FeNC SACs by ultrasonic atomization in conjunction with pyrolysis and calcination. (B) Evaluation of electrochemical performance on FeNC, FeNC SACs, and 20% Pt/C catalysts. (a) Linear sweep voltammetry (LSV) curves, (b) comparison of halfwave potential ( $E_{1/2}$ ) and kinetic current density ( $J_k$ ), (c) Tafel plots, (d) Nyquist plots obtained by electrochemical impedance spectroscopy (EIS), (e) relative current density–time curves of FeNC SACs and 20 wt% Pt/C catalysts at 0.6 V with methanol injection, and (f) relative current density–time curves at 0.6 V for 36 000 seconds (10 hours). Source: Ma et al. [121].

LDH preserve OER and HER bifunctions in the same reaction medium, having been studied intensively. It was also found that CoFe LDH, CoMn LDH, CuCoO nanowires, FeCoOH, Cu@CoFe, and NiMo nanorods have OER and HER bifunction. Recently, Inamdar et al. developed another robust non-precious copper–iron (CuFe) bimetallic composite that can be used as a highly efficient bifunctional catalyst for overall water splitting in an alkaline medium. Their catalyst exhibits outstanding OER and HER activity, and very low OER and HER overpotentials (218 and 158 mV, respectively) are necessary to attain a current density of 10 mA/cm<sup>2</sup> [144]. When used in a two-electrode water electrolyzer system for overall water splitting, it not only achieves high durability (even at a very high current density of 100 mA/cm<sup>2</sup>) but also reduces the potential required to split water into oxygen and hydrogen at 10 mA/cm<sup>2</sup> to 1.64 V for 100 hours of continuous operation.

Many 2D materials, such as MoS<sub>2</sub>, have been studied for catalyzing the HER of water, showing great promise as a cost-effective alternative to Pt even though the current catalytic efficiency is still worse than that of Pt. [146, 147] Cao and coworkers recently report a strategy to enable the catalytic activity of monolayer MoS<sub>2</sub> films that are even better than that of Pt via engineering the interface interaction of the monolayer with supporting substrates [146]. The monolayer films were grown with CVD processes and controlled to have an optimal density (7–10%) of sulfur vacancies. They found that the catalytic activity of MoS<sub>2</sub> could be affected by substrates in two ways: forming an interfacial tunneling barrier with MoS<sub>2</sub> and modifying the chemical nature of MoS<sub>2</sub> via charge transfer. Thus, excellent catalytic activities at the monolayer MoS<sub>2</sub> films can be obtained by using substrates that can provide n-doping to MoS<sub>2</sub> and form low interfacial tunneling barriers with MoS<sub>2</sub> (e.g. Ti). The catalytic performance may be further boosted to be even better than Pt by crumpling the films on Ti-coated flexible polymer substrates, as the Tafel slope of the film is substantially decreased with the presence of crumpling-induced compressive strain.

The monolayer MoS<sub>2</sub> films show no degradation in catalytic performance after being continuously tested for over two months.

Another kind of thin-film electrode for water splitting, which can be a potential candidate to replace the precious metal catalyst-based electrode is based on TM-based nanocatalysts. They have been attracting great attention due to their low cost and abundance as compared with those precious-metal-based catalysts, but their low performance (particularly insufficient activity) still remains a challenge. Many strategies (e.g. size, shape, hierarchical structure, and composition control) have been developed to improve their performance in the past few years. One example of the progress in these TM-based nanocatalysts is the 4 nm Mn<sub>3</sub>O<sub>4</sub> nanoparticles (NPs) developed recently by Nam and coworkers [148]. It is confirmed that the overall increase in the active surface area is distinctly related to the superb catalytic activity of the 4 nm Mn<sub>3</sub>O<sub>4</sub> NPs by comparing them with those 8 nm species. To further enhance the OER performance, the interface interaction between the catalysts and the support should be optimized. As expected, introducing of Ni foam substrate can indeed maximize the entire number of the NPs participating in OER. An outstanding electrocatalytic activity for OER was obtained using the 4 nm Mn<sub>3</sub>O<sub>4</sub>/Ni foam electrode, with an overpotential of 395 mV at a current density of 10 mA/cm<sup>2</sup> under neutral conditions (0.5 M phosphate buffer saline (PBS), pH 7).

## 1.5 Thin Films and Coatings for Key Sources and Ecological Environment of Earth

Water is the first key source for all organisms on Earth [149, 150]. Even though 71% of Earth's surface is covered by ocean, only 2.53% of water is fresh water that is not the uniform distribution in the earth. Many areas are very deficient of fresh water, such as the Sahara and many countries in Africa, the Middle-East areas, California and Nevada of the USA, North and Northwest District of China, and most isolated islands. Water has played a key role in social and national security in the history of human beings [149, 150]. In order to resolve the freshwater shortage, governments have invested lots in many huge projects, such as the partly-finished South-to-North Water Diversion Project in China. While the USA has paid attention to desalination technology, to obtain fresh water from the ocean or brackish water has been on the watch by the USA government to address the water shortage in California since the 1950s [151–153]. The reverse osmosis technology based on highly efficient permeability membranes (e.g. reverse osmosis thin-film composite membrane) emerges as the times require insight from the semipermeability of animal bladders [153]. Dr. Song has systemically summarized the progress of permeable membranes in his dissertation in 2000 [153]. With the rapid development of new separation concept, novel membrane materials science, advanced fabrication technology, and automatic control engineering in the past two decades, great progress has been achieved in membrane science and separation technology [151, 154–162]. Because of varieties of advantages of select osmotic membrane technologies (e.g. the high selectivity [based on molecule weight, geometry, affinity, and configuration] and

permeability, the possibility non-phase transformation or controlled phase change during separation, noncontact and temperature difference between products and feeds, the possibility for nonthermal exchange process, and low operation cost), lots of permeable membranes or related separation technologies have been invented for the separation, purification, and concentration of desired products in almost all industry involving the fluids (gas or liquid), particularly foods, pharmacy, gas separation, chemical engineering, petroleum refining, chemistry synthesis, environment protection, and waste recycling and reutilization [149, 152, 154–165].

When using a membrane to separate materials, the efficiency of the separation is limited by how fast the gas or liquid passes through the membrane and by how selective it is. Thinner membranes usually allow for faster flow rates but are usually less selective and strength. In order to increase the flux without loss of selectivity, many technologies and membrane materials have been invented in the past decade. The most impressive progress may be the incorporation of the magic two-dimensional (2D) materials [166–171] and/or varieties of carbon allotropes (i.e. porous carbon, graphene, carbon nanotube) into the thin-film composite membranes that have greatly addressed the trade-off between selectivity and permeability, one of the main issues in the membrane materials development [149, 154, 156, 164, 172, 173]. Particularly, graphene – with great mechanical strength, chemical stability, and inherent impermeability – offers a unique 2D system with which to realize this membrane and study the mass transport. One sophisticated perforating strategy to maintain the selectivity without losing permeability was successfully developed by Celebi et al. [174], which entails the precisely drilling holes of controlled diameter in a graphene sheet about two layers thick, up to a few million pores with narrowly distributed diameters between less than 10 nm and 1  $\mu\text{m}$ . For such a thin membrane, the primary barriers to separation come from entrance and exit from the holes and not from the motion through the membrane, which can have highly efficient mass transfer across physically perforated double-layer graphene but still maintain a high selectivity. The measured transport rates are in agreement with predictions of 2D transport theories. Attributed to its atomic thicknesses, these porous graphene membranes show higher permeance of gas, liquid, and water vapor far in excess of those shown by finite-thickness membranes, highlighting the ultimate permeation these 2D membranes can provide. Varieties of graphene-based (including GO: partially oxidized and stacked sheets of graphene [175]) thin-film composite membranes have been developed, which can possibly address this issue and has reached the separation resolution of molecule/ion sieving ability in the selectivity [149, 156, 164, 172, 173]. Two-dimensional materials such as graphene and graphene oxide membranes (GOMs) [175],  $\text{MoS}_2$ , can provide ultrathin, high-flux, and energy-efficient membranes possible with ångström-scale channels with atomically flat walls for precise ionic and/or molecular sieving in aqueous solutions [166, 169–171, 176, 177] and gas-phase (e.g.  $\text{H}_2$  or He) separation [167, 168, 178]. These materials have been made into varieties of thin films and coating of different microstructures and layers, showing potential in a variety of applications, including water desalination and purification [179–181] and gas and ion separation [160, 167, 168, 178, 182–184]

However, there are still lots of work to do in the controlled modification of 2D materials for highly efficient permeable membranes to overcome their intrinsic limitation, for example, graphene, unlike the pores of carbon nanotube membranes that have fixed sizes, while the pores of GOMs and the interlayer spacing between GO sheets are of variable size [185], and it is difficult to reduce the interlayer spacing sufficiently to exclude small ions and to maintain this spacing against the tendency of GOMs to swell when immersed into aqueous solution [186]. These challenges hinder the potential ion filtration applications of GOMs. In 2017, Fang and coworkers [160] developed a cationic control strategy to tune the interlayer spacing of GOMs with ångström (Å) precision using  $K^+$ ,  $Na^+$ ,  $Ca^{2+}$ ,  $Li^+$ , or  $Mg^{2+}$  ions. Membrane spacings controlled by one type of cation can efficiently and selectively exclude other cations that have larger hydrated volumes. Using this strategy, they fabricated centimeter-scale GOMs on ceramic supports experimentally, achieving facile and precise control of the interlayer spacing, with a precision of down to 1 Å, and corresponding ion rejection, through the addition of one kind of cation (e.g.  $K^+$ ) [160]. This method is based on the understanding of the strong noncovalent hydrated cation- $\pi$  interactions between hydrated cations and the aromatic ring, indicating that other ions could be used to produce a wider range of interlayer spacings [160]. Generally, this method provokes a step toward graphene-oxide-based thin-film applications, such as water desalination and gas purification, solvent dehydration, lithium-based batteries and supercapacitors, and molecular sieving.

Freshwater flux and energy consumption are two important benchmarks for the membrane desalination process. Nanoporous carbon composite membranes have been developed by Sheng's group in April 2018 [156], which comprise a layer of porous carbon fiber structures grown on a porous ceramic substrate, showing 100% desalination and a freshwater flux of 3–20 times higher than existing polymeric membranes. Thermal accounting experiments demonstrated that the carbon composite membrane could save over 80% of the latent heat consumption. Conventional technology for the purification of organic solvents requires massive energy consumption, as well as to reduce such expending calls for efficient filtration membranes capable of high retention of large molecular solutes and high permeance for solvents. In September 2019, Tang's group [161] reported a surface-initiated polymerization strategy through C–C coupling reactions for preparing conjugated microporous polymer (CMP) membranes of high resistance to organic solvents due to the all-rigid conjugated systems in the backbone of the membranes. The prepared 42-nm-thick CMP membranes supported on polyacrylonitrile substrates exhibited excellent retention of solutes and broad-spectrum nanofiltration in both nonpolar hexane and polar methanol, the permeance for which reaches 32 and 221/m<sup>2</sup>/h/bar, respectively.

Besides this issue, antifouling may forever be one of the main issues during the long-term operation, particularly biofouling, which will result in the flux reduction, the deterioration of selectivity, and/or the broken of membranes, finally leading to a short lifetime of membranes [163, 187]. Many novel methods have been invented in resolving the membrane fouling problem [163, 187].

Another interesting innovative technology in clean water production using membrane separation technology should be the bionic-plant-leaf-inspired sunlight-driven purifier for high-efficiency clean water production [155]. It is well-known that the transpiration and guttation process of natural vascular plant leaves can produce tons of clean water via osmotic pressure differences powered by sunlight. Inspired by this transpiration and guttation process, a sunlight-driven purifier is designed for high-efficiency water purification and production. This sunlight driven purifier is constructed by a negative temperature response poly(*N*-isopropylacrylamide) (PNIPAm) (PN) hydrogel anchored onto a superhydrophilic melamine foam skeleton, and a layer of PNIPAm modified graphene (PG) filter membrane coated outside. Molecular dynamics simulation and experimental results show that the superhydrophilicity of the relatively rigid melamine skeleton significantly accelerates the swelling/deswelling rate of the poly (isopropylacrylamide) (PNIPAm) (PN) and PNIPAm modified graphene (PG) -filter (PNPG-F) purifier. Under one sun, this rational engineered structure offers a collection of 4.2 kg/m<sup>2</sup>/h and an ionic rejection of >99% for a single poly (*N*-isopropylacrylamide) (PNIPAm) (PN) and PNIPAm modified graphene (PG) (PNPG) filter from brine feed via the cooperation of transpiration and guttation. It is envisioned that such a high-efficiency sunlight-driven system could have great potential applications in diverse water treatments.

Besides the freshwater resource crisis, another great challenge before people may be the deterioration of our ecology and environment, particularly the atmospheric pollution that is mainly resulted from more and more toxic gas releasing and greenhouse gas emissions. One strategy to reduce the pollution of these gases is to resource them, such as reducing CO<sub>2</sub> into ethylene or CO into methanol. Lots of resource technologies have been developed in the past decades. The electrochemical reduction reaction of CO<sub>2</sub> (CO<sub>2</sub>RR) may be the most promising method to fulfill this issue by transferring CO<sub>2</sub> into chemical resources (e.g. urea, merlon, ethylene) or syngases (e.g. methane, methanol) [188–191]. The key to this technology is to find the catalysts of high efficiency and low cost to replace the expensive precious-metal-based species. Carbon-based solid-state catalyst materials containing small amounts of nitrogen and TM have emerged as a selective and cost-efficient alternative to noble metal catalysts for the direct electrochemical reduction of CO<sub>2</sub> into CO, formic acid, or methane. Recently, Ana Sofia Varela and Peter Strasser summarized the recent progress of MNC catalysts for the CO<sub>2</sub>RR [190]. There is a growing interest in MNC materials as catalysts for the CO<sub>2</sub>RR, given their remarkably high activities and selectivity toward CO formation, their ability to form “beyond CO” hydrocarbons, and their affordable synthesis methods. Studies have shown that the metal center plays a crucial role in determining the catalytic performance of the material. For instance, Fe has been shown to produce CO selectively at low overpotentials and to have the ability to reduce CO further to traces of CH<sub>4</sub> [192], whereas Ni-containing materials have been reported as highly selective toward CO production. They have mentioned that the density functional theory-guided experimental studies could provide the elucidation of key experimental parameters and molecular descriptors. The catalytic performance in

the presence of different metals can be rationalized based on the binding energy between the metal center and the reaction intermediates, which might promote the activity and selectivity of the MNC catalysts for future highly efficient nonprecious catalyst development. In this review, it is further pinpointed that there are still several key scientific issues that deserved to be deeply studied in this emerging field. One is the nature of the active sites. Understanding the role of all the possible active sites will be crucial for designing optimal catalysts containing highly active and selective catalytic sites. One needs new instruments for this active site study. The second issue is how to optimize the reaction conditions since they play a major role in the catalytic process besides the catalyst structure and composition. For instance, working in acidic pH favors the competing process of the HER reducing the selectivity toward the CO<sub>2</sub>RR. Therefore, it would be desired to work in neutral or alkaline pH values to have a highly selective process. Another important factor to consider is the accessibility of the active sites. When working with a highly active catalyst, the CO<sub>2</sub>RR can be limited by the transport of CO<sub>2</sub> to the active sites. In this regard, the structure of carbon support plays a crucial role in the transport of CO<sub>2</sub> through the catalyst layer. The low CO<sub>2</sub> solubility, however, is also a major reason for mass transport limitations. Therefore, in general, we have to determine the reaction conditions that are practical for the catalytic screening based on their industrial application. For an instance, the use of gas diffusion electrodes (GDEs) can help to overcome the pH limitations by having the gas stream and electrolyte stream separated by the electrode, which preserve a more realistic assessment of the catalytic performance of a given material for the CO<sub>2</sub>RR at a large scale if the screening is carried out using GDE electrolyzers.

## 1.6 Thin Films and Coatings for Biomedical Engineering and Life Science

Polymers and biomass form an integral part of our existence and everything that surrounds us – from the basic building blocks of life constituting of proteins, nucleic acids, and polysaccharides to the commercial products obtained from automobile, construction and transportation industries, plastic toys and tools, reading glasses, etc. Most of these materials are composed of a combination of one or more materials to form polymer composites. And a film made of a polymer as a matrix or a carrier is referred to as a polymer-based film. Due to its excellent composite properties and processing diversity, polymer films have been increasingly employed in production and are gradually applied to defense, transportation, aerospace, marine engineering, and other fields (e.g. thin films for artificial intelligence). Many functional polymers, particularly biodegradable species, have been fabricated into thin films and coatings of special surface patterns as biosensors or other kinds of functions (antibacterial, antifouling) for biomedical engineering and life science [187, 193–196]. In this book, the polymer-based films for artificial intelligence, selective permeable thin films and their applications for water purification and wastewater treatment, biomass-derived functional films, and anti-marine corrosion coatings

have been summarized in details in Chapters 13, 14, 15, and 19, respectively. Here, we will briefly introduce some other interesting progress of polymeric thin films and coatings for biomedical engineering and life science.

One of them is the thin films formed via self-assembly of biocompatible or biodegradable hyperbranched polymers (HBPs), which have lots of cytomimetic applications, summarized by Jin et al. [197]. The HBPs have demonstrated great potential to be used as model membranes to mimic cellular behaviors, such as fusion, fission, and cell aggregation via self-assembly into varieties of sizes, shapes, and structures, such as honeycomb structures. Natural honeycomb structures are usually observed in plants or beehives with a columnar and hexagonal array of hollow cells formed between thin vertical walls. Now, many synthetic honeycomb films can be prepared through the self-assembly of homopolymers, linear block copolymers, and star copolymers according to a breath-figure technique. The amphiphilic HBPs could self-assemble into honeycomb-like microporous films by the slow evaporation of a chloroform solution of the precursors in a humid atmosphere. The pore diameter could be controlled easily by adjusting the casting volume, polymer concentration, molecular weight, and so forth.

Another interesting progress is the relation between the polymers and nanoparticles for biomedicines, such as the antibacterial dressing [193], the formation the surface patterning of nanoparticles with polymer patches as biosensors [198], and artificial electronic skins [199]. Patterning of colloidal particles with chemically or topographically distinct surface domains (patches) has attracted intense research interest [198]. Surface-patterned particles act as colloidal analogs of atoms and molecules, serve as model systems in studies of phase transitions in liquid systems, behave as “colloidal surfactants,” and function as templates for the synthesis of hybrid particles. Although the fabrication of micrometer- and submicrometer-sized patchy colloids has been matured, it is still difficult to prepare the patched surface patterns from inorganic nanoparticles of tens of nanometers. These inorganic nanoparticles exhibit size- and shape-dependent optical, electronic, and magnetic properties, and their assemblies show new collective properties [200]. Nanoparticle patterning is usually limited to the generation of two-patch nanoparticles [201–203] and nanoparticles with surface ripples [204] or a “raspberry” [205] surface morphology. Choueiri et al. invented a method to precisely prepare nanoparticle surface patterning utilizing thermodynamically driven segregation of polymer ligands from a uniform polymer brush into surface-pinned micelles following a change in solvent quality [198]. Patch formation is reversible but can be permanently preserved using a photocrosslinking step, which would suppress nanoparticle assembly and enable the utilization of solutions with a higher nanoparticle concentration, thereby increasing the yield of patchy nanoparticles. This methodology offers the ability to control the dimensions of patches, their spatial distribution, and the number of patches per nanoparticle. These patchy nanocolloids have potential applications in fundamental research, the self-assembly of nanomaterials, diagnostics, sensing, and colloidal stabilization [198]. Patterning of multicomponent nanoparticles and the self-assembly of patterned nanoparticles into complex, hierarchical structures can be further explored by some other kinds of surface modification methods, such as

surface grafting. Furthermore, due to the progress in the synthesis of nanoparticles of different sizes, shapes, and structures, the proposed strategy should enable fundamental studies of polymer segregation on surfaces with large curvatures or surfaces with multiple curvatures.

Silk protein is one of the promising biodegradable and biocompatible materials as substrates for electronic devices in artificial intelligence, such as on-skin and implantable electronic devices. However, its intrinsic brittleness and poor thermal stability limit its applications. Recently, robust and heat-resistant silk fibroin composite membranes (SFCMs) are synthesized by mesoscopic doping of regenerated silk fibroin via the strong interactions between silk fibroin (SF) and polyurethane invented by Guo and coworkers [199]. The schemed process to fabricate the integrated protein-based electronic skin (PBES) via SFCMs is illustrated in Figure 1.9 [199].

Some traditional micromachining techniques, such as inkjet printing, can be used to print flexible circuits on such protein substrates (Figure 1.9a). The obtained SFCMs can endure the tensile test more than 200% and the thermal resistance up to 160 °C. Based on this substrate, Ag nanofibers (NFs) and Pt NFs networks have been successfully embedded onto both sides of the SFCMs as heaters and

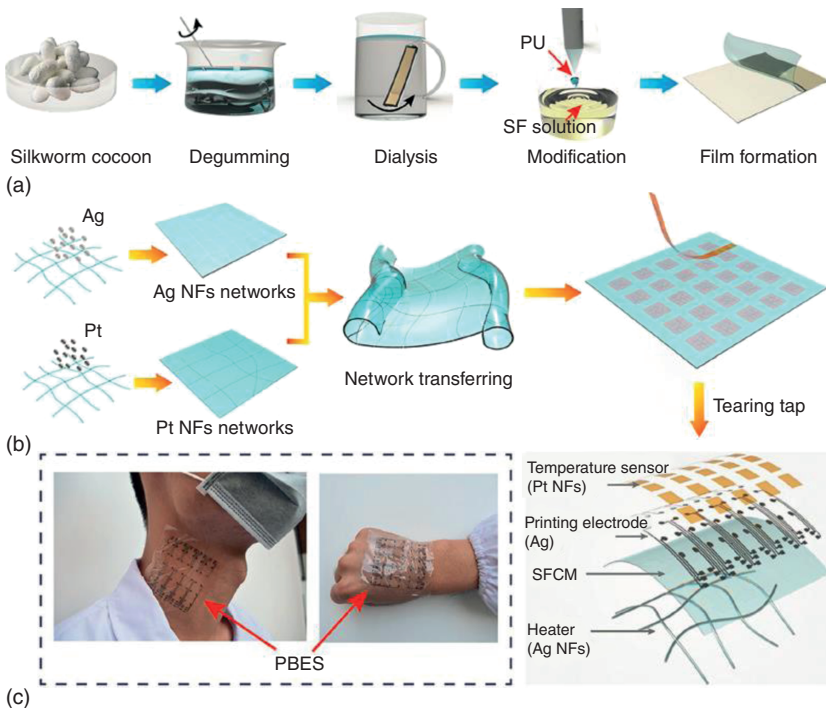


**Figure 1.9** Fabrication of PBES based on SFCM. (a) Schematic illustration of the preparation of flexible transparent SFCM; (b) schematic illustration of the fabrication of PBES realizing heating and temperature detection; (c) photographic images of the PBES attaching to the human neck and hand closely. Source: Huang et al. [199].

temperature sensors, respectively (Figure 1.9b,c). The integrated PBES exhibits high thermal stability and temperature sensitivity ( $0.205\%/^{\circ}\text{C}$ ). Heating and temperature distribution detection are realized by array-type PBES, contributing to potential applications in dredging the blood vessel for alleviating arthritis (Figure 1.9c). This PBES is both inflammation-free and air-permeable, which can directly be laminated onto human skin for long-term thermal management.

Single-molecule detection is vital for basic research and practical applications in nanobiotechnology and nanomedicine [206]. Fabrication techniques that yield sensors with repeatable performance are critical to the sensitive detection and precise control of biomolecules [194, 207]. One way is to fabricate bio-wells as small as possible to only save one or several biomolecules [194]; another way to exert control on a biomolecule is to use guiding structures to impose a change in shape or behavior on the molecule of interest [194, 206, 207]. Nanopore or nanocavity thin films provide nanoscale channels or femtoliter volume, which are now well established as possible single-biomolecule sensors label-free or not, which hold great promise as sensing elements in diagnostic and gene sequencing applications [194, 206, 207]. Nanopore technology is particularly attractive for DNA sequencing because of its potential advantages, which include long reads and high speed [206]. Single nanopores can be used for highly sensitive detection of DNA by threading the polymer through the pore, blocking some of the electrical current that normally would pass through the pore. Usually, the nanopore or cavity thin films can be fabricated by traditional e-beam and RIE processes [194, 206, 207]. However, this promise has been limited by the expensive, labor-intensive, and low-yield methods used to fabricate low-noise and precisely sized pores or cavities [207].

Nanoscale preconfinement of DNA is shown to reduce the variation of passage times through solid-state nanopores. Preconfinement is previously achieved by forming a femtoliter-sized cavity capped with a highly porous layer of nanoporous silicon nitride (NPN). This cavity is formed by sealing an NPN nanofilter membrane against a substrate chip using water vapor delamination. However, this method of fabrication cannot keep a consistent spacing between the filter and solid-state nanopore due to thermal fluctuations and wrinkles in the membrane, nor can it be fabricated on thousands of individual devices reliably. To overcome these issues, McGrath and coworkers advanced a new process to fabricate the femtoliter cavity monolithically using a selective xenon difluoride ( $\text{XeF}_2$ ) etch to hollow out a polysilicon (poly-Si) spacer sandwiched between silicon nitride ( $\text{SiN}_x$ ) layers, as schemed in Figure 1.10 [194]. These monolithically fabricated cavities behave identically to their counterparts formed by vapor delamination, exhibiting similar translocation passage time variation reduction and folding suppression of DNA without requiring extensive manual assembly. The ability to form nanocavity sensors with nanometer-scale precision and to reliably manufacture them at scale using batch wafer processing techniques will find numerous applications, including motion control of polymers for single-molecule detection applications, filtering of dirty samples prior to nanopore detection, and simple fabrication of single-molecule nanobioreactors.

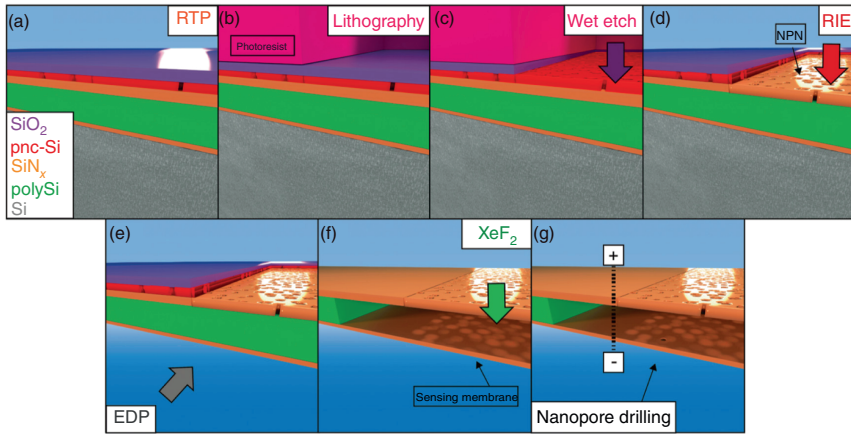


**Figure 1.10** Monolithically created femtoliter cavity process flow. (a) pnc-Si is formed as a hard mask over the thin-film stack with RTP and (b) lithographically patterned. (c) The exposed capping SiO<sub>2</sub> layer is removed using an ammonium bifluoride wet etch. (d) The nanopore pattern is transferred into the prefilter layer using an RIE process (SF<sub>6</sub> + O<sub>2</sub>), forming NPN in the desired cavity geometry. (e) After an EDP etch to create access to the backside of the device, (f) the femtoliter cavity is formed through the use of XeF<sub>2</sub>, which enters through the NPN and hollows out the poly-Si layer between the NPN and the sensing SiN<sub>x</sub> membrane (15 nm). The remaining pnc-Si and SiO<sub>2</sub> are also concurrently removed. (g) Finally, the cavity is wetted, and then, a sensing nanopore is formed in the sensing membrane layer via CBD. Source: Madejski et al. [194].

To address the problem for the nanopore membrane fabrication, Goto et al. have been developing a controlled dielectric breakdown process to enable rapid nanopore fabrication since 2016, and now, this process can offer an upgraded method to fabricate nanopore membranes for DNA-sequencing technology [206, 208]. Recently, Waugh et al. proposed another low-cost and scalable solid-state nanopore fabrication method, termed controlled breakdown (CBD), which is rapidly becoming the method of choice for fabricating solid-state nanopores. Since its initial development, nanopore research groups around the world have applied and adapted the CBD method in a variety of ways, with varying levels of success that present their accumulated knowledge of nanopore fabrication by CBD, including a detailed description of the instrumentation, software, and procedures required to reliably fabricate low-noise and precisely sized solid-state nanopores with a yield of >85% in less than one hour. The general platform for this method is illustrated by Waugh et al. [207]. Unlike traditional beam-based nanopore fabrication technologies, the methods presented here are low-cost and low technical barriers for the fabrication of nanoscale pores in thin solid-state membranes, which is accessible for non-experts.

In addition, Song and coworkers, also developed an alternative method to fabricate nanopore membranes of controlled sizes, shapes, and substrates, named as template transfer nanoimprinting [18, 20, 22, 47, 209], which will be summarized in Chapters

10 and 11 of this book. We believed that industrial applications that take advantage of this sensing modality include DNA sequencing DNA barcoding and investigating single-molecule capture and transport shall be realized soon with the progress of the marriage of the nanofabrication technique to the biomedical engineering.

The third promising progress of thin films or coatings for biomedical and life science exists in some functional thin films formed by 2D materials, such as graphene. As a new nanomaterial, graphene has shown great promise in drug delivery, cancer therapy, and other nano-biomedical techniques due to its unique microstructures and mechanical and electronic properties. Graphene has been used in the fabrication of other kinds of permeable membranes with enhanced permeability [210], such as reverse osmosis membranes that can preserve great potential in the purification of wastewater and soft water produced by desalination of ocean water for life science, which were summarized in Chapter 14 of this book comprehensively with other kinds of permeable membranes. Recently, one of the promising methods based on the electric properties of GO composites is to introduce into the separation membrane to control the water permeability using an electric field, which is very important in the healthcare technologies related to the controlled water permeability in capillaries or membranes (e.g. artificial skins) [211]. Previous attempts to control water permeation through membranes (mainly polymeric ones) have concentrated on modulating the structure of the membrane and the physicochemical properties of its surface by varying the pH, temperature, or ionic strength [212, 213]. Electrical control over water transport is an attractive alternative. Many micrometer-thick GOMs have been invented for ultrafast permeation of water [178, 214] and molecular sieving [169, 215], with the potential for industrial-scale production. To achieve electrical control over water permeation, Nair and coworkers created conductive filaments in the GOMs via controllable electrical breakdown in 2018 [211]. The scheme of how to fabricate the E-controlled GO composite membranes was given as follows [211]. The GO multilayered membranes were first deposited in a well formed by a polymer molding method supported on a porous silver substrate [211]. The metal/GO/metal sandwich structures were then formed by depositing a thin ( $\approx 10$  nm) gold (Au) film on top of the GOM prepared on the porous silver (Ag) substrate. One of the metal-GO-metal sandwich membranes was attached to the Polyethylene Terephthalate (PET) sheet. Such a thin layer of gold is sufficiently porous and shows the discontinuities and voids in a 10-nm gold thin film on a GOM. Therefore, the coated gold layer does not change the permeation properties of the membranes. However, the water permeability depended on the thickness of the gold layer and the concentration of hydrogen ions and hydroxide ions. Then, the electric field can be imposed between the silver layer and the gold layer to fulfill the E-controlled permeability testing. The electric field that concentrates around these current-carrying filaments ionizes water molecules inside graphene capillaries within the GOMs, which impedes water transport. Thus, the water permeation can be precisely controlled from ultrafast permeation to complete blocking. This work opens up an avenue for developing smart membrane technologies for artificial biological systems, tissue engineering, and filtration.

## 1.7 Thin Films and Coatings for National Defense and Homeland Security

There are many sophisticated thin films and coatings used in varieties of instruments and equipment for the national defense and homeland security. In this book, we will emphasize some distinctive key thin films and coatings for aeronautics, information security, and marine voyages. The armor coatings for tanks or armored cars will not be discussed in this book.

As for coatings for aeronautics, the most key coatings are the thermal barrier coatings (TBCs) and radar stealth coatings. TBCs are a kind of ceramic layers grown or deposited on the superalloy substrates constructing the turbine blades in the “heart” of aircraft or the jet engine in the propulsion system. They function as the thermal and corrosion protection layers of the superalloy substrates in the combustion chamber of jet engines free from high corrosion and oxidizing gas spraying at high temperatures ( $\sim 2000^\circ\text{C}$  or higher) and high speed (sometimes several times of sound velocity). Readers can refer to Chapter 19 of this book for detailed microstructures and fabrication processes of varieties of TBCs. In order to evade the detection by the hostile radar system, stealth coatings for electromagnetic (EM) waves have to be equipped on the top surface of air vehicles together with the whole structure stealth design, particularly for fighters and strategic/long-range bombers. These coatings are usually called radar-absorbing materials made of magnetic nanomaterials and/or carbon-based porous materials, which are discussed in detail in Chapter 18 of this book.

The modern information communication, particularly for long-distance communication, is mainly based on the encoding-emission-transmission-receiving-decoding technologies of EM waves up to now even though the quantum communication that is still a long time for commercialization has emerged. Therefore, electromagnetic interference (EMI) compatibility coatings are still the key technique for the information security related to the national defense and homeland safety. The microstructure and material design of these coatings is also based on the EM-wave-matter interaction, which will be summarized in Chapter 18 together with the radar stealth coatings.

In the marine voyages, the most key coatings are possibly those coatings related to the anti-marine corrosion coatings and the anechoic coating systems in the sonar (sound navigation and ranging) systems for the underwater vehicles and surface ships, which are intimately related to the national coastal defense safety and the maritime trade profit security. The detailed analyses on these coatings are summarized in Chapters 16 and 17, respectively. Here, we just want to mention one interesting progress in the hydrogel microphones for stealthy underwater listening related to the future marine source exploration [216].

Vehicles traveling in oceans, particularly for those underwater vehicles (e.g. submarines, unmanned undersea vehicles), usually navigate based on their sonar systems to monitor flow velocities and sound waves to navigate, to identify hostile objects, to track ocean currents and surface waves, and to communicate with each other [217, 218]. However, the conventional ceramic-piezoelectric (PZT)-based

sonar systems suffer from a large acoustic impedance mismatch with water, causing them to be easily detected by hostile vehicles during the current era of stealthy navigation because they efficiently reflect incoming acoustic signals [216, 219, 220]. In addition, the detection efficiency of PZT-based acoustic sensors is relatively poor at low frequencies [216]. Alternatively, suspended thin membranes of poly(vinylidene fluoride) [221] or graphene stretched over air cavities [222] have been proposed as microphones to afford a higher sensitivity than PZT [223], but these configurations introduce even larger mismatch in acoustic impedance between the device (air) and water [216].

Considering the advances in acoustic metamaterial cloaking, which greatly attenuates incoming acoustic signals, thereby concealing submarine bodies from sonar detection, a ceramic PZT detector or cavity-based microphone, which is necessarily kept outside of this “invisibility cloak,” remains a strong acoustic reflector [224–226]. In contrast to a rigid solid such as ceramics or a low-density compliant medium such as air, hydrogels have almost perfect acoustic impedance matching with water [216]. Polar functional groups from the backbone or side chains allow hydrogels to absorb a large amount of liquid into three-dimensional polymer networks without leaking. Different from dielectric capacitors, where their capacitance is governed by the distance between two parallel electrodes [227], hydrogel capacitors derive their capacitance from electrical double layers (EDLs) [216, 228]. With the excellent acoustic impedance match to water, a hydrogel capacitor seems to be a promising acoustic transducer. The problem, however, is that the low compressibility of water means that an EDL capacitor would have low sensitivity to pressures. In addressing this limitation, a suitable sensor can be made by incorporating a deformable network of metal nanoparticles (MNPs) into the hydrogel. The MNP network makes the capacitor highly sensitive to mechanical stimuli through a coupling between the deformation of the MNP network and the ion modulation. As a result, this MNP–hydrogel capacitor is able to detect deformation, pressure, and acoustic waves. The key to this hydrophone is the fabrication of the MNP–hydrogel network. Figure 1.11a schemes the synthesis process of the MNP–hydrogel network.

In step 1, hydrogel is presoaked in an aqueous bath of  $\text{AgNO}_3$  (e.g. 10 mM) [216]. Then, hydrogel is sandwiched and biased between an amorphous silicon (a-Si) and an ITO plate (step 2). After that, photoactivated a-Si reduces  $\text{Ag}^+$  into  $\text{Ag}^0$  nanoparticles at specific locations (step 3). Finally, MNP–hydrogel is soaked in a copper sulfate bath to prepare a smooth and robust layer of surface electrodes (step 4). Figure 1.11b,c gives the photograph of the patterned Ag nanoparticles in the skin depth of the hydrogel, the high-resolution SEM image, and the schematic of the dendritic MNP network inside the hydrogel.

Furthermore, hydrogel microphones can be fabricated by the cavity-free coatings via integrating the easily deformable MNP–hydrogel network in the hydrogel matrix, as highlighted in Figure 1.12a–g [216]. Figure 1.12a shows an example of a  $9 \text{ mm}^2$  hydrogel microphone fabricated by forming an MNP network consisting of dendritic structures 2–3 mm in size and being buried inside the soft and translucent hydrogel matrix (Figure 1.12b). This MNP–hydrogel microphone was electrically biased at 1 V and submerged in water (Figure 1.12c), where it picked

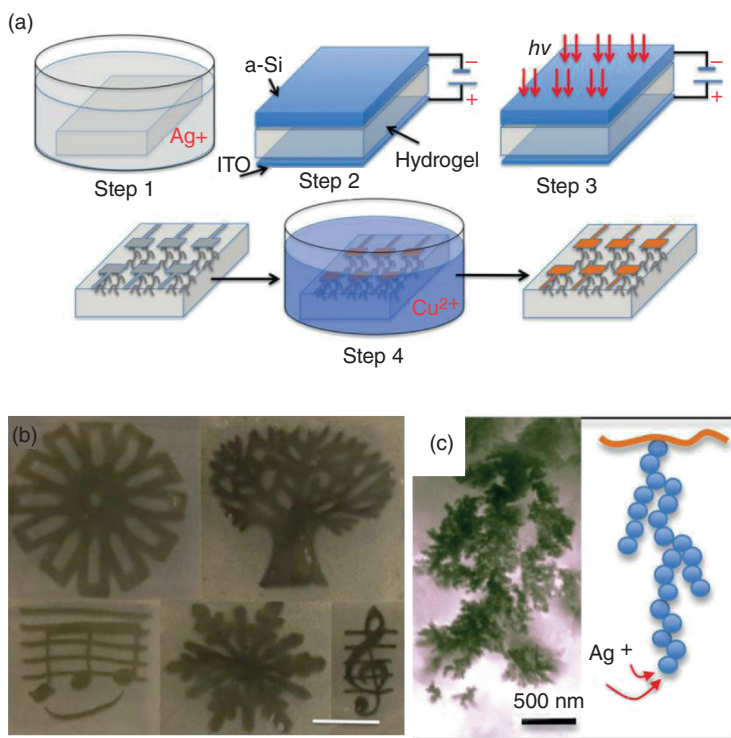


**Figure 1.11** Fabrication of hydrogel microphones. (a) Steps to fabricate a deformable network of metal nanoparticles (MNPs) and surface electrode. (b) Photos of patterned Ag nanoparticles in the skin depth of the hydrogel. Scale bar, 3.0 mm. (c) High-resolution SEM image and schematic of a dendritic MNP network inside the hydrogel. Source: Gao et al. [216].

up acoustic waves and produced a signal 30 dB stronger at low frequencies than a commercial hydrophone (Figure 1.12d). Moreover, the hydrogel microphone has a wide frequency response, up to 2 kHz (Figure 1.12e), and has a pronounced directional sensitivity perpendicular to the sensor surface (Figure 1.12f). MNP–hydrogel (Figure 1.12g: solid lines) responds to a static pressure of 5.4 kPa with more than four times in relative capacitance change or seven to eight times in capacitance change than MNP-free device (Figure 1.12g: dashed lines). Since MNPs can be densely implanted as inclusions and can even be arranged in coherent arrays, the general performance testing results suggest that this microphone can detect static loads and air breezes from different angles, as well as underwater acoustic signals from 20 Hz to 3 kHz at amplitudes as low as 4 Pa [216]. Unlike dielectric capacitors or cavity-based microphones that respond to stimuli by deforming the device in thickness directions, this hydrogel device responds with a transient modulation of electric double layers, resulting in an extraordinary sensitivity (217 nF/kPa or 24  $\mu\text{C}/\text{N}$  at a bias of 1.0 V) without using any signal amplification tools [216]. Due to their perfect acoustic impedance matching with water, ultrasensitive for low-frequency acoustic waves, the nanomaterial–hydrogel-based hydrophones have currently become an

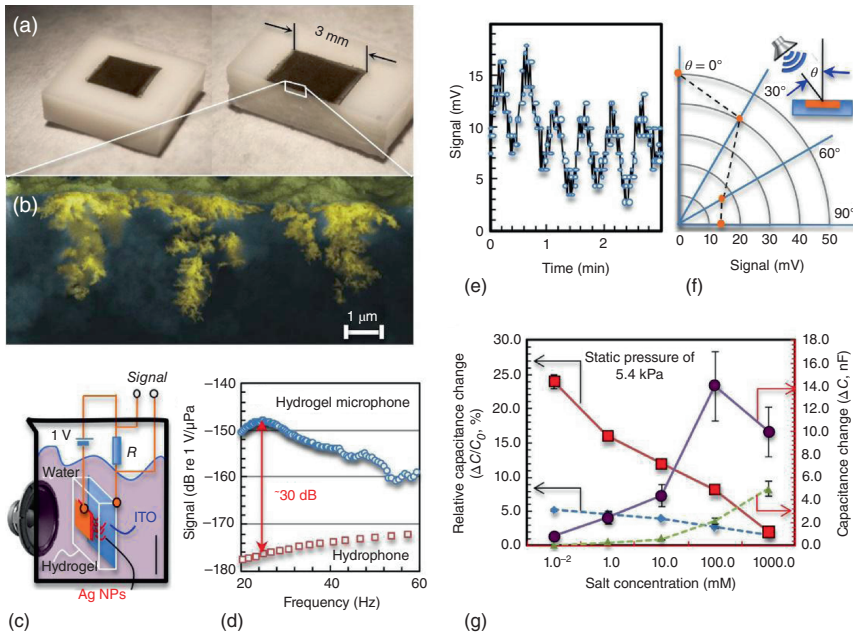


**Figure 1.12** Highlight of hydrogel microphone. (a) Photos (full view and sliced) and (b) scanning electron microscopy (SEM) image of the hydrogel membrane implanted with a patch ( $3 \times 3 \text{ mm}^2$ ) of silver dendrites (highlighted yellow). (c) Setup and circuit using the membrane as a microphone. (d) Better performance of the hydrogel microphone at low frequencies than a commercial device (hydrophone). (e) Hydrogel microphone is capable of detecting underwater sound at 2 kHz and (f) at all angles. Note: the  $0^\circ$  orientation is for the top surface of the microphone facing toward the loudspeaker. (g) MNP-hydrogel (solid lines) responds to a static pressure of 5.4 kPa with more than four times in relative capacitance change or seven to eight times in capacitance change than MNP-free device (dashed lines). The relative errors of direct current (DC) and  $\text{DC}/C_0$  for MNP-hydrogel are, respectively, 21–25% and 3.5–4.5%. For MNP-free hydrogel, the relative errors of DC and  $\text{DC}/C_0$  are, respectively, 13.0–13.5% and 3.0–4.0%. Source: Gao et al. [216].

exciting area for developing hydrophones for potential antiscouting sonar [229, 230] or ultrasensitive stretchable pressure sensors [231, 232].

## Acknowledgments

This chapter was supported by the NSFC-BRICS STI Framework Program (No. 51861145309), the National Natural Science Foundation of China (No. 51971029), the National S&T Major Project (No. 2018ZX10301201), the “All English teaching demonstration course construction project of University of Science and Technology Beijing” (No. KC2015QYW06, 2016), the “1125” Zhihui Zhengzhou Talent project of Henan province (Fund No. in USTB: 39080070), the “100 talent plan” fund of Fujian province (Fund No. in USTB: 39080067), and the development of a highly sensitive magneto-optical biomolecular sensor experimental prototype (Fund No. in USTB: 2019-0649) by Hangzhou Ruidi Biotechnology Co. Ltd.

## List of Abbreviations

2D	two-dimensional
3D	three-dimensional
AEMs	atom electronic mechanics
AIBs	aluminum-ion batteries
AND	agree nor disagree
BDA	butanediamine
BIF	build-in field
CBD	controlled breakdown
CCD	charge-coupled device
C-dots	carbon quantum dots
CIGS	copper indium gallium selenide
CMOS	complementary metal-oxide semiconductor
CMP	conjugated microporous polymer
CMR	colossal magnetoresistance
CO <sub>2</sub> RR	reduction reaction of CO <sub>2</sub>
CVD	chemical vapor deposition
DJ	Dion Jacobson
EDLs	electrical double layers
EG	expansion reduced graphene
EM	electromagnetic
EMI	electromagnetic interference
ESSs	energy storage systems
ETL-free PSCs	electron transport layer-free perovskite solar cells
F4TCNQ	2,3,5,6-tetrafluoro-7,7,8,8-tetracyanoquinodimethane
FCs	fuel cells
FEA	pentafluorophenylethyl ammonium
FET	field emission transistor
FOLEDs	foldable OLEDs
GDEs	gas diffusion electrodes
GMR	giant magnetoresistance
GNRs	graphene nanoribbons
GO	graphene oxide
GON	germanium-on-nothing
Gp	graphene
GPU	graphics processing unit
h-BN (hBN)	hexagonal boron nitride
HBP	hyperbranched polymers
HER	hydrogen evolution reaction
HR-TEM	high-resolution transmission electron microscopy
HTM	hole-transporting material
ITO	indium tin oxide
LDH	layered bimetallic hydroxide
LED	laser emission diodes

LSC	luminous solar concentrator
MAPbI <sub>3</sub>	methylammonium lead iodide
MBE	molecular beam epitaxy
MEMs	microelectronic mechanics
MNC	metal–nitrogen–carbon
MNPs	metal nanoparticles
MO	magneto-optical
MOSFET	metal-oxide-semiconductor field-effect transistor
MoTe <sub>2</sub>	molybdenum ditelluride
NAND	neither agree nor disagree
NCPV	National Center for Photovoltaics
NEMs	nanoelectronic mechanics
NFs	nanofibers
NPN	nanoporous silicon nitride
NPs	nanoparticles
NREL	National Renewable Energy Laboratory
OER	oxygen evolution reaction
OLED	organic light emitting diode
ORR	oxygen reduction reaction
PBES	protein-based electronic skin
PCE	power conversion efficiency
PDA	propanediamine
PEM	proton-exchange membrane
PFE	polar ferroelectric
PG	PNIPAm modified graphene
P-Hg	black phosphorus
PHJ	plane heterojunctions
PLQY	photoluminescence quantum yield
PN	poly( <i>N</i> -isopropylacrylamide) (PNIPAm)
PNPL	halide perovskite nanoflake
PSCs	perovskite solar cells
poly-Si	polysilicon
PV	photovoltaic
PZT	piezoelectric
QAHE	quantum anomalous hall effect
QW	quantum well
rGO	reduced graphene oxide
RTG	thermoelectric power generator
SACs	single-atom catalysts
SEIs	solid electrolyte interfaces
SEM	scanning electronic microscope
SFCMs	silk fibroin composite membranes
SiN <sub>x</sub>	silicon nitride
SMEMs	single-molecule electronic mechanics
SSCs	single-site catalysts

TBCs	thermal barrier coatings
TE	thermoelectric
TM	transition metal
TMDs	transition metal dichalcogenides
TMR	tunneling magnetoresistance
TSCs	tandem solar cells
UCD	Universal Communication Device™
XeF <sub>2</sub>	xenon difluoride
XOR	exclusive-OR

## References

- 1 Kroemer, H. (2001). Nobel Lecture: quasidelectric fields and band offsets: teaching electrons new tricks. *Reviews of Modern Physics* 73: 783.
- 2 Alferov, Z.I. (2001). Nobel lecture: the double heterostructure concept and its applications in physics, electronics, and technology. *Reviews of Modern Physics* 73: 767.
- 3 Gao, W., Zhu, X., Zheng, F., et al. (2018). A possible candidate for triply degenerate point fermions in trigonal layered PtBi<sub>2</sub>. *Nature Communications* 9: 3249. <https://doi.org/10.1038/s41467-018-05730-3>.
- 4 Xiang, R., Inoue, T., Zheng, Y., et al. (2020). One-dimensional van der Waals heterostructures. *Science* 367: 537–542.
- 5 Schwierz, F. (2010). Graphene transistors. *Nature Nanotechnology* 5, 487–496.
- 6 Ge, S., Zhao, Z., Pai, J.-H. et al. (2016). Highly sensitive, wearable, durable strain sensors, and stretchable conductors using graphene/silicon rubber composites. *Advanced Functional Materials* 26: 7614–7625.
- 7 Yang, H., Yao, X., Yuan, L. et al. (2019). Strain-sensitive electrical conductivity of carbon nanotube-graphene-filled rubber composites under cyclic loading. *Nanoscale Research Letters* 11: 578–586.
- 8 Yin, F., Lu, H., Pan, H., et al. (2019). Highly sensitive and transparent strain sensors with an ordered array structure of AgNWs for wearable motion and health monitoring. *Scientific Reports* 9: 1–10.
- 9 Han, S., Chand, A., Araby, S., et al. (2019). Thermally and electrically conductive multifunctional sensor based on epoxy/graphene composite. *Nanotechnology* 31: 075702.
- 10 Pan, C., Fu, Y., Wang, J., et al. (2018). Vertical transistors: analog circuit applications based on ambipolar graphene/MoTe<sub>2</sub> vertical transistors (Adv. Electron. Mater. 3/2018). *Advanced Electronic Materials* 4: 1870015.
- 11 Qi, X.-L. and Zhang, S.-C. (2010). The quantum spin Hall effect and topological insulators. *Physics Today* 63: 33–38.
- 12 Kong, D. and Cui, Y. (2011). Opportunities in chemistry and materials science for topological insulators and their nanostructures. *Nature Chemistry* 3: 845–849.

- 13 Rienks, E.D.L., Wimmer, S., Sánchez-Barriga, J., et al. (2019). Large magnetic gap at the Dirac point in  $\text{Bi}_2\text{Te}_3/\text{MnBi}_2\text{Te}_4$  heterostructures. *Nature* 576: 423–428. <https://doi.org/10.1038/s41586-019-1826-7>.
- 14 Cao, Y., Fatemi, V., Demir, A., et al. (2018). Correlated insulator behaviour at half-filling in magic-angle graphene superlattices. *Nature* 556: 80–84. <https://doi.org/10.1038/nature26154>.
- 15 Rhodes, D., Chae, S.H., Ribeiro-Palau, R., and Hone, J. (2019). Disorder in van der Waals heterostructures of 2D materials. *Nature Materials* 18: 541–549. <https://doi.org/10.1038/s41563-019-0366-8>.
- 16 Wang, E., Lu, X., Ding, S., et al. (2016). Gaps induced by inversion symmetry breaking and second-generation Dirac cones in graphene/hexagonal boron nitride. *Nature Physics* 12: 1111–1115. <https://doi.org/10.1038/nphys3856>.
- 17 Liu, Y., Weiss, N.O., Duan, X., et al. (2016). Van der Waals heterostructures and devices. *Nature Reviews Materials* 1: 16042. <https://doi.org/10.1038/natrevmats.2016.42>.
- 18 Zhang, W., Wang, Y., Wang, Q. et al. (2018). The surface and interface engineering multi-layered nanopore films for enhanced Fabry–Pérot interferences. *The Journal of Physical Chemistry C* 122: 29457–29463.
- 19 Knyazev, G.A., Kapralov, P.O., Gusev, N.A. et al. (2018). Magnetoplasmonic crystals for highly sensitive magnetometry. *ACS Photonics* 5: 4951–4959. <https://doi.org/10.1021/acsp Photonics.8b01135>.
- 20 Zhang, W., Li, J., Ding, X., et al. (2017). Tunable magneto-optical Kerr effects of nanoporous thin films. *Scientific Reports* 7: 2888.
- 21 Diaz-Valencia, B.F., Mejía-Salazar, J.R., Oliveira, O.N. et al. (2017). Enhanced transverse magneto-optical Kerr effect in magnetoplasmonic crystals for the design of highly sensitive plasmonic (bio)sensing platforms. *ACS Omega* 2: 7682–7685.
- 22 Zhang, W., Wang, Q., Zhao, C., and Song, Y. (2019). The optical cavity enhanced magneto-optical Kerr effect signals of AAO/Al-based CoFeB nanostructure arrays. *Optics Communications* 437: 44–49.
- 23 Assouar, B., Liang, B., Wu, Y., et al. (2018). Acoustic metasurfaces. *Nature Reviews Materials* 3: 460–472. <https://doi.org/10.1038/s41578-018-0061-4>.
- 24 Fan, Y., Shen, N.-H., Zhang, F., et al. Photoexcited graphene metasurfaces: significantly enhanced and tunable magnetic resonances. *ACS Photonics* <https://doi.org/10.1021/acsp Photonics.8b00057>.
- 25 Fasold, S., Linß, S., Kawde, T. et al. (2018). Disorder-enabled pure chirality in bilayer plasmonic metasurfaces. *ACS Photonics* 5: 1773–1778.
- 26 Collins, J.T., Hooper, D.C., Mark, A.G. et al. (2018). Second-harmonic generation optical rotation solely attributable to chirality in plasmonic metasurfaces. *ACS Nano*: 10.1021/acsnano.8b00601.
- 27 Lee, H., Jung, M., Kim, M., et al. (2018). Acoustically sticky topographic metasurfaces for underwater sound absorption. *The Journal of the Acoustical Society of America* 143: 1534–1547.
- 28 Langfeldt, F. and Gleine, W. (2019). Improved sound transmission loss of glass wool with acoustic metamaterials. *Proceeding of the 26th ICSV*, pp. 7–11.

- 29 Talirz, L., Ruffieux, P., and Fasel, R. (2016). On-surface synthesis of atomically precise graphene nanoribbons. *Advanced Materials* 28: 6222–6231.
- 30 Verlhac, B., Bachellier, N., Garnier, L., et al. (2019). Atomic-scale spin sensing with a single molecule at the apex of a scanning tunneling microscope. *Science* 366: 623–627.
- 31 Jiang, Y., Chen, Z., Han, Y., et al. (2018). Electron ptychography of 2D materials to deep sub-ångström resolution. *Nature* 559: 343–349.
- 32 Xiong, X., Huang, M., Hu, B., et al. (2020). A transverse tunnelling field-effect transistor made from a van der Waals heterostructure. *Nature Electronics* 3: 106–112. <https://doi.org/10.1038/s41928-019-0364-5>.
- 33 Liu, Y., Huang, Y., and Duan, X. (2019). Van der Waals integration before and beyond two-dimensional materials. *Nature* 567: 323–333.
- 34 Yan, R., Khalsa, G., Vishwanath, S., et al. (2018). GaN/NbN epitaxial semiconductor/superconductor heterostructures. *Nature* 555: 183–189.
- 35 Cao, Y., Fatemi, V., Fang, S., et al. (2018). Unconventional superconductivity in magic-angle graphene superlattices. *Nature* 556: 43–50.
- 36 Lin, Z., Liu, Y., Halim, U., et al. (2018). Solution-processable 2D semiconductors for high-performance large-area electronics. *Nature* 562: 254–258.
- 37 Gibaja, C., Rodriguez-San-Miguel, D., Ares, P. et al. (2016). Back cover: few-layer antimonene by liquid-phase exfoliation (*Angew. Chem. Int. Ed.* 46/2016). *Angewandte Chemie* 55: 14470–14470.
- 38 Dong, A., Chen, J., Vora, P.M. et al. (2010). Binary nanocrystal superlattice membranes self-assembled at the liquid–air interface. *Nature* 466: 474–477.
- 39 Goerbig, M., Montambaux, G., and Piéchon, F. (2014). Measure of Diracness in two-dimensional semiconductors. *EPL (Europhysics Letters)* 105: 57005.
- 40 Cai, J., Ruffieux, P., Jaafar, R., et al. (2010). Atomically precise bottom-up fabrication of graphene nanoribbons. *Nature* 466: 470–473.
- 41 Gröning, O., Wang, S., Yao, X., et al. (2018). Engineering of robust topological quantum phases in graphene nanoribbons. *Nature* 560: 209–213. <https://doi.org/10.1038/s41586-018-0375-9>.
- 42 Son, Y.W., Cohen, M.L., and Louie, S.G. (2006). Energy gaps in graphene nanoribbons. *Physical Review Letters* 97: 216803.
- 43 Cao, T., Zhao, F., and Louie, S.G. (2017). Topological phases in graphene nanoribbons: junction states, spin centers, and quantum spin chains. *Physical Review Letters* 119: 076401.
- 44 Song, Y., Nallathamby, P.D., Huang, T. et al. (2010). Correlation and characterization of 3D morphological dependent localized surface plasmon resonance spectra of single silver nanoparticles using dark-field optical microscopy and AFM. *The Journal of Physical Chemistry C* 114: 74–81.
- 45 Song, Y. (2011). *Controlled Fabrication of Noble Metal Nanomaterials via Nanosphere Lithography and their Optical Properties*. INTECH Open Access Publisher.
- 46 Zhang, W., Liu, Z., Belotelov, V.I. et al. (2018). The magnetic properties of CoFeB and CoFeB/Ag nanodot arrays fabricated by a template transfer imprinting method. *Thin Solid Films* 660: 301–305.

- 47 Song, Y., Yin, W., Wang, Y.H., et al. (2014). Magneto-plasmons in periodic nanoporous structures. *Scientific Reports* 4: 4991. <https://doi.org/10.1038/srep04991>.
- 48 Song, Y., Zhang, Z., Elsayed-Ali, H.E., et al. (2011). Identification of single nanoparticles. *Nanoscale* 3: 31–44.
- 49 Kumar, G., Tang, H.X., and Schroers, J. (2009). Nanomoulding with amorphous metals. *Nature* 457: 868–872.
- 50 Jeong, E.G., Kwon, J.H., Kang, K.S. et al. (2019). A review of highly reliable flexible encapsulation technologies towards rollable and foldable OLEDs. *Journal of Information Display*: 1–14.
- 51 Rogers, J., Bao, Z., and Lee, T.-W. (2019). Wearable bioelectronics: opportunities for chemistry. *Accounts of Chemical Research* 52: 521–522.
- 52 Sugimoto, A., Ochi, H., Fujimura, S., et al. (2004). Flexible OLED displays using plastic substrates. *IEEE Journal of Selected Topics in Quantum Electronics* 10: 107–114.
- 53 Park, J.-S., Chae, H., Chung, H.K., and Lee, S.I. (2011). Thin film encapsulation for flexible AM-OLED: a review. *Semiconductor Science and Technology* 26: 034001.
- 54 Zhang, W., Zhao, C., Chen, Z., et al. (2020). Ultrasensitive surface-enhanced raman scattering (SERS) nanopore arrayed silver thin film substrates for R6G detection. *RSC Advances* 10: 23908–23915.
- 55 Ye, C., Chao, D., Shan, J., et al. (2020). Unveiling the advances of 2D materials for Li/Na-S batteries experimentally and theoretically. *Matter* 2: 323–344.
- 56 Seebeck, T. and Magnetische, J. (1826). Polarisation der Metalle und Erze durch Temperatur-Differenz. *Annalen der Physik* 82: 133–160.
- 57 Peltier, J.C.A. (1834). New experiments on the heat effects of electric currents. *Annales de Chimie Physique* 56: 371–386.
- 58 Satterthwaite, C. and Ure, R. Jr., (1957). Electrical and thermal properties of  $\text{Bi}_2\text{Te}_3$ . *Physical Review A* 108: 1164–1170.
- 59 Goldsmid, H.J. (1955). XXVII. Thermoelectric applications of semiconductors. *International Journal of Electronics* 1: 218–222.
- 60 Dismukes, J., Ekstrom, L., Steigmeier, E. et al. (1964). Thermal and electrical properties of heavily doped Ge–Si alloys up to 1300 K. *Journal of Applied Physics* 35: 2899–2907.
- 61 Allen, A.W. (1997). Detector handbook. *Laser Focus World* 33: S15.
- 62 He, J. and Tritt, T.M. (2010). *Thermal-to-Electrical Energy Conversion from the Nanotechnology Perspective* (ed. J. Garcia-Martinez), 47–77. John Wiley and Sons, Ltd.. <https://doi.org/10.1002/9783527629299.ch3>.
- 63 Bansal, P., Vineyard, E., and Abdelaziz, O. (2011). Advances in household appliances - a review. *Applied Thermal Engineering* 31: 3748–3760.
- 64 Zhao, L.-D., Lo, S.-H., Zhang, Y., et al. (2014). Ultralow thermal conductivity and high thermoelectric figure of merit in SnSe crystals. *Nature Catalysis* 508: 373–377.
- 65 Yang, J., Xi, L., Qiu, W., et al. (2016). On the tuning of electrical and thermal transport in thermoelectrics: an integrated theory–experiment perspective. *npj Computational Materials* 2: 1–17.

- 66 Tan, G., Hao, S., Cai, S., et al. (2019). All-scale hierarchically structured p-type PbSe alloys with high thermoelectric performance enabled by improved band degeneracy. *Journal of the American Chemical Society* 141: 4480–4486.
- 67 Zhang, J., Song, L., and Iversen, B.B. (2019). Insights into the design of thermoelectric  $\text{Mg}_3\text{Sb}_2$  and its analogs by combining theory and experiment. *npj Computational Materials* 5: 76.
- 68 Sales, B.C., Mandrus, D., and Williams, R.K. (1996). ChemInform abstract: filled skutterudite antimonides: a new class of thermoelectric materials. *Science* 272: 1325–1328.
- 69 Butt, S., Liu, Y.-C., Lan, J.-L., et al. (2014). High-temperature thermoelectric properties of La and Fe co-doped Ca–Co–O misfit-layered cobaltites consolidated by spark plasma sintering. *Journal of Alloys and Compounds* 588: 277–283.
- 70 Hao, S., Dravid, V.P., Kanatzidis, M.G., and Wolverton, C.J. (2019). Computational strategies for design and discovery of nanostructured thermoelectrics. *npj Computational Materials* 5: 58.
- 71 Morelli, D.T. (2017). Chapter 57. Thermoelectric materials. In: *Handbook of Electronic and Photonic Materials*, Chapter 57, Part E (eds. S. Kasap and P. Capper), 1379–1395. Springer.
- 72 Tritt, T.M., Böttner, H., and Chen, L. (2008). Thermoelectrics: direct solar thermal energy conversion. *MRS Bulletin* 33: 366–368.
- 73 Hu, Y., Song, L., Chen, Y., and Huang, W. (2019). Two-terminal perovskites tandem solar cells: recent advances and perspectives. *Solar RRL* 3, <https://doi.org/10.1002/solr.201900080>.
- 74 Grinberg, I., West, D.V., Torres, M., et al. (2013). Perovskite oxides for visible-light-absorbing ferroelectric and photovoltaic materials. *Nature Catalysis* 503: 509–512.
- 75 Sum, T.C. and Mathews, N. (2014). Advancements in perovskite solar cells: photophysics behind the photovoltaics. *Energy & Environmental Science* 7: 2518–2534.
- 76 Roldán-Carmona, C., Malinkiewicz, O., Soriano, A., et al. (2014). Flexible high efficiency perovskite solar cells. *Energy & Environmental Science* 7: 994–997.
- 77 Green, M.A., Ho-Baillie, A., and Snaith, H.J. (2014). The emergence of perovskite solar cells. *Nature Photonics* 8: 506–514.
- 78 Dualeh, A., Moehl, T., Tétreault, N., et al. (2014). Impedance spectroscopic analysis of lead iodide perovskite-sensitized solid-state solar cells. *ACS Nano* 8: 362–373.
- 79 Elumalai, N.K., Mahmud, M.A., Wang, D., and Uddin, A. (2016). Perovskite solar cells: progress and advancements. *Energies* 9: 861.
- 80 Rose, G. (1839). *De Novis Quibusdam Fossilibus Quae in Montibus Uraliis Inveniuntur*. AG Schade.
- 81 Zhu, X. (2016). The perovskite fever and beyond. *Accounts of Chemical Research* 49: 355–356.
- 82 Wu, W.-Q., Wang, Q., Fang, Y., et al. (2018). Molecular doping enabled scalable blading of efficient hole-transport-layer-free perovskite solar cells. *Nature Communications* 9: 1–8.

- 83 Rong, Y., Hu, Y., Mei, A., et al. (2018). Challenges for commercializing perovskite solar cells. *Science* 361: eaat8235.
- 84 Zheng, Y., Niu, T., Qiu, J., et al. (2019). Oriented and uniform distribution of Dion–Jacobson phase perovskites controlled by quantum well barrier thickness. *Solar RRL* 3: 1900090.
- 85 Liu, Y., Akin, S., Pan, L., et al. (2019). Ultrahydrophobic 3D/2D fluoroarene bilayer-based water-resistant perovskite solar cells with efficiencies exceeding 22%. *Science Advances* 5: eaaw2543.
- 86 Benetti, D., Jokar, E., Yu, C.-H., et al. (2019). Hole-extraction and photostability enhancement in highly efficient inverted perovskite solar cells through carbon dot-based hybrid material. *Nano Energy* 62: 781–790.
- 87 Zhang, C.C., Wang, Z.K., Yuan, S., et al. (2019). Polarized ferroelectric polymers for high-performance perovskite solar cells. *Advanced Materials* 31: 1902222.
- 88 Braukyla, T., Xia, R., Daskeviciene, M., et al. (2019). Inexpensive hole-transporting materials derived from Tröger’s base afford efficient and stable perovskite solar cells. *Angewandte Chemie* 131: 11388–11394.
- 89 Liu, T., Luo, Z., Chen, Y. et al. (2019). A nonfullerene acceptor with a 1000 nm absorption edge enables ternary organic solar cells with improved optical and morphological properties and efficiencies over 15%. *Energy & Environmental Science* 12: 2529–2536.
- 90 Chen, Y., Liu, T., Hu, H. et al. (2018). Modulation of end groups for low-bandgap nonfullerene acceptors enabling high-performance organic solar cells. *Advanced Energy Materials* 8: 1801203. <https://doi.org/10.1002/aenm.201801203>.
- 91 Fan, Q., Zhu, Q., Xu, Z. et al. (2018). Chlorine substituted 2D-conjugated polymer for high-performance polymer solar cells with 13.1% efficiency via toluene processing. *Nano Energy* 48: 413–420.
- 92 Cui, Y., Yao, H., Zhang, J., et al. (2019). Over 16% efficiency organic photovoltaic cells enabled by a chlorinated acceptor with increased open-circuit voltages. *Nature Communications* 10: 1–8.
- 93 Park, S., Simon, J., Schulte, K. L., et al. (2019). Germanium-on-nothing for epitaxial liftoff of GaAs solar cells. *Joule* 3: 1782–1793.
- 94 Cai, L. and Yu, G. (2019). Recent advances in growth and modification of graphene-based energy materials: from chemical vapor deposition to reduction of graphene oxide. *Small Methods* 3: 1900071.
- 95 Liu, Z., You, P., Xie, C. et al. (2016). Ultrathin and flexible perovskite solar cells with graphene transparent electrodes. *Nano Energy* 28: 151–157.
- 96 Li, Z., Johnston, A., Wei, M., et al. (2020). Solvent-solute coordination engineering for efficient perovskite luminescent solar concentrators. *Joule* 4: 631–643.
- 97 Huang, L., Zhang, D., Bu, S., et al. (2020). Synergistic interface energy band alignment optimization and defect passivation toward efficient and simple-structured perovskite solar cell. *Advanced Science* 7: 1902656. <https://doi.org/10.1002/advs.201902656>.
- 98 Polman, A., Knight, M., Garnett, E.C. et al. (2016). Photovoltaic materials: present efficiencies and future challenges. *Science* 352: aad4424.

- 99 Tiedje, T., Yablonovitch, E., Cody, G.D., and Brooks, B.G. (1984). Limiting efficiency of silicon solar cells. *IEEE Transactions on Electron Devices* 31: 711–716.
- 100 De Vos, A. (1980). Detailed balance limit of the efficiency of tandem solar cells. *Journal of Physics D: Applied Physics* 13: 839.
- 101 Strandberg, R. (2015). Detailed balance analysis of area de-coupled double tandem photovoltaic modules. *Applied Physics Letters* 106: 033902.
- 102 Futscher, M.H. and Ehrler, B. (2016). Efficiency limit of perovskite/Si tandem solar cells. *ACS Energy Letters* 1: 863–868.
- 103 Lamanna, E., Matteocci, F., Calabrò, E., et al. (2020). Mechanically stacked, two-terminal graphene-based perovskite/silicon tandem solar cell with efficiency over 26%. *Joule* 4: 865–881. <https://doi.org/10.1016/j.joule.2020.01.015>.
- 104 Shi, L. and Zhao, T. (2017). Recent advances in inorganic 2D materials and their applications in lithium and sodium batteries. *Journal of Materials Chemistry A* 5: 3735–3758.
- 105 Kühne, M., Boerrnert, F., Fecher, S., et al. (2018). Reversible superdense ordering of lithium between two graphene sheets. *Nature* 564: 234–239. <https://doi.org/10.1038/s41586-018-0754-2>.
- 106 Nguyen, D.D., Hsiao, C.H., Su, T.Y., et al. (2019). Bioinspired networks consisting of spongy carbon wrapped by graphene sheath for flexible transparent supercapacitors. *Communications Chemistry* 2: 137. <https://doi.org/10.1038/s42004-019-0238-9>.
- 107 Yu, Z., Jiao, S., Li, S. et al. (2019). Flexible stable solid-state Al-ion batteries. *Advanced Functional Materials* 29, <https://doi.org/10.1002/adfm.201806799>.
- 108 Winter, M. and Besenhard, J.O. (2011). III. Materials for alkali metal batteries. In: *Handbook of Battery Materials* (eds. C. Daniel and J.O. Besenhard), 433–478. Wiley-VCH.
- 109 Kaskhedikar, N.A. and Maier, J. (2009). Lithium storage in carbon nanostructures. *Advanced Materials* 21: 2664–2680.
- 110 Zheng, H., Meng, Y.S., and Zhu, Y. (2015). Frontiers of in situ electron microscopy. *MRS Bulletin* 40: 12–18.
- 111 Qian, D., Ma, C., More, K.L. et al. (2015). Advanced analytical electron microscopy for lithium-ion batteries. *NPG Asia Materials* 7: e193.
- 112 Liu, X.H., Liu, Y., Kushima, A., et al. (2012). In situ TEM experiments of electrochemical lithiation and delithiation of individual nanostructures. *Advanced Energy Materials* 2: 722–741.
- 113 Shao-Horn, Y., Croguennec, L., Delmas, C. et al. (2003). Atomic resolution of lithium ions in LiCoO<sub>2</sub>. *Nature Materials* 2: 464–467.
- 114 Oshima, Y. and Murakami, Y. (2017). Challenges for lithium detection (special issue). *Microscopy* 66: 1–61.
- 115 Reimer, L. and Kohl, H. (2008), Springer Series in Optical Sciences (eds. W.T. Rhodes, A. Adibi, T. Asakura, et al.). New York: Springer, ISSN: 0342-4111.
- 116 Linck, M., Hartel, P., Uhlemann, S. et al. (2016). Chromatic aberration correction for atomic resolution TEM imaging from 20 to 80 kV. *Physical Review Letters* 117: 076101.

- 117 Enoki, T., Suzuki, M., and Endo, M. (2003). *Graphite Intercalation Compounds and Applications*. Oxford University Press.
- 118 Li, Z., Gadipelli, S., Li, H., et al. (2020). Tuning the interlayer spacing of graphene laminate films for efficient pore utilization towards compact capacitive energy storage. *Nature Energy* 5: 160–168. <https://doi.org/10.1038/s41560-020-0560-6>.
- 119 Stamenkovic, V.R., Strmcnik, D., Lopes, P.P., and Markovic, N.M. (2016). Energy and fuels from electrochemical interfaces. *Nature Materials* 16: 57–69. <https://doi.org/10.1038/nmat4738>.
- 120 Chu, S., Cui, Y., and Liu, N. (2016). The path towards sustainable energy. *Nature Materials* 16: 16–22. <https://doi.org/10.1038/nmat4834>.
- 121 Ma, J., Wang, L., Deng, Y. et al. (2020). Mass production of high-performance single atomic FeNC electrocatalysts via sequenced ultrasonic atomization and pyrolysis process. *Science China Materials*, <https://doi.org/10.1007/s40843-020-1464-6>.
- 122 Chen, Y., Ji, S., Zhao, S., et al. (2018). Enhanced oxygen reduction with single-atomic-site iron catalysts for a zinc-air battery and hydrogen-air fuel cell. *Nature Communications* 9: 5422. <https://doi.org/10.1038/s41467-018-07850-2>.
- 123 Tiwari, J.N., Tiwari, R.N., Singh, G., and Kim, K.S. (2013). Recent progress in the development of anode and cathode catalysts for direct methanol fuel cells. *Nano Energy* 2: 553–578. <https://doi.org/10.1016/j.nanoen.2013.06.009>.
- 124 Shao, M., Chang, Q., Dodelet, J.-P., and Chenitz, R. (2016). Recent advances in electrocatalysts for oxygen reduction reaction. *Chemical Reviews* 116: 3594–3657. <https://doi.org/10.1021/acs.chemrev.5b00462>.
- 125 Mori, K., Sano, T., Kobayashi, H., and Yamashita, H. (2018). Surface engineering of a supported PdAg catalyst for hydrogenation of CO<sub>2</sub> to formic acid: elucidating the active Pd atoms in alloy nanoparticles. *Journal of the American Chemical Society* 140: 8902–8909. <https://doi.org/10.1021/jacs.8b04852>.
- 126 Yan, Z., He, G., Shen, P. K. et al. (2014). MoC–graphite composite as a Pt electrocatalyst support for highly active methanol oxidation and oxygen reduction reaction. *Journal of Materials Chemistry A* 2: 4014. <https://doi.org/10.1039/c3ta14251e>.
- 127 Yao, Y., Hu, S., Chen, W. et al. (2019). Engineering the electronic structure of single atom Ru sites via compressive strain boosts acidic water oxidation electrocatalysis. *Nature Catalysis* 2: 304–313. <https://doi.org/10.1038/s41929-019-0246-2>.
- 128 Ma, J., Tong, X., Wang, J. et al. (2019). Rare-earth metal oxide hybridized PtFe nanocrystals synthesized via microfluidic process for enhanced electrochemical catalytic performance. *Electrochimica Acta* 299: 80–88. <https://doi.org/10.1016/j.electacta.2018.12.132>.
- 129 Wang, Z., Fan, H., Liang, H., et al. (2017). Microfluidic synthesis and characterization of FePtSn/C catalysts with enhanced electro-catalytic performance for direct methanol fuel cells. *Electrochimica Acta* 230: 245–254. <https://doi.org/10.1016/j.electacta.2017.01.1590013-4686>.

- 130 Ott, S., Orfanidi, A., Schmies, H., et al. (2020). Ionomer distribution control in porous carbon-supported catalyst layers for high-power and low Pt-loaded proton exchange membrane fuel cells. *Nature Materials* 19: 77–85. <https://doi.org/10.1038/s41563-019-0487-0>.
- 131 Wang, J., Ye, H., and Song, Y. (2018). In-situ reaction-growth of PtNiX nanocrystals on supports forenhanced electrochemical catalytic oxidation of ethanol via continuous flow microfluidic process. *Electrochimica Acta* 278: 149–155.
- 132 Glösen, A., Dionigi, F., Paciok, P., et al. (2019). Dealloyed PtNi-core-shell nanocatalysts enable significant lowering of Pt electrode content in direct methanol fuel cells. *ACS Catalysis* 9: 3764–3772. <https://doi.org/10.1021/acscatal.8b04883>.
- 133 Dionigi, F., Weber, C.C., Primbs, M., et al. (2019). Controlling near-surface Ni composition in octahedral PtNi(Mo) nanoparticles by Mo doping for a highly active oxygen reduction reaction catalyst. *Nano Letters* 19: 6876–6885. <https://doi.org/10.1021/acs.nanolett.9b02116>.
- 134 Sun, Y., Silvioli, L., Sahraie, N.R., et al. (2019). Activity–selectivity trends in the electrochemical production of hydrogen peroxide over single-site metal–nitrogen–carbon catalysts. *Journal of the American Chemical Society* 141: 12372–12381. <https://doi.org/10.1021/jacs.9b05576>.
- 135 Garcon, M., Bakewell, C., Sackman, G.A., et al. (2019). A hexagonal planar transition-metal complex. *Nature* 574: 390–393. <https://doi.org/10.1038/s41586-019-1616-2>.
- 136 Song, Y., Hart, K.T., and Dooley, K.M. (2004). Waste-reducing catalysis for acylation of a secondary amine: synthesis of DEET. *Catalysis Letters* 98: 69–75. <https://doi.org/10.1007/s10562-004-7933-5>.
- 137 Song, Y., Hart, K.T., and Dooley, K.M. (2016). Waste-reducing catalytic oxidation of m-xylene to m-toluic acid. *Catalysis Letters* 146: 1213–1220.
- 138 Jasinski, R. (1964). A new fuel cell cathode catalyst. *Nature* 201: 1212–1213. <https://doi.org/10.1038/2011212a0>.
- 139 Huang, K., Zhang, L., Xu, T., et al. (2019). 60°C solution synthesis of atomically dispersed cobalt electrocatalyst with superior performance. *Nature Communications* 10: 606. <https://doi.org/10.1038/s41467-019-08484-8>.
- 140 Liu, X., Wang, L., Yu, P. et al. (2018). A stable bifunctional catalyst for rechargeable zinc-air batteries: iron-cobalt nanoparticles embedded in a nitrogen-doped 3D carbon matrix. *Angewandte Chemie* 57: 16166–16170. <https://doi.org/10.1002/anie.201809009>.
- 141 Huang, X., Zhang, Y., Shen, H., et al. (2018). N-doped carbon nanosheet networks with favorable active sites triggered by metal nanoparticles as bifunctional oxygen electrocatalysts. *ACS Energy Letters* 3: 2914–2920. <https://doi.org/10.1021/acsenerylett.8b01717>.
- 142 Sun, T., Tian, B., Lu, J., and Su, C. (2017). Recent advances in Fe (or Co)/N/C electrocatalysts for the oxygen reduction reaction in polymer electrolyte membrane fuel cells. *Journal of Materials Chemistry A* 5: 18933–18950. <https://doi.org/10.1039/c7ta04915c>.

- 143** Nie, Y., Li, L., and Wei, Z. (2015). Recent advancements in Pt and Pt-free catalysts for oxygen reduction reaction. *Chemical Society Reviews* 44: 2168–2201. <https://doi.org/10.1039/c4cs00484a>.
- 144** Inamdar, A.I., Chavan, H.S., Hou, B., et al. (2020). Electrochemical water splitting: a robust nonprecious CuFe composite as a highly efficient bifunctional catalyst for overall electrochemical water splitting. *Small* 16: 1905884.
- 145** Chen, Z., Song, Y., Cai, J., et al. (2018). Tailoring the d band centers enables Co<sub>4</sub>N nanosheets to be highly active for hydrogen evolution catalysis. *Angewandte Chemie International Edition* 130: 5170–5174. <https://doi.org/10.1002/anie.201801834>.
- 146** Li, G., Chen, Z., Li, Y., et al. (2020). Engineering substrate interaction to improve hydrogen evolution catalysis of monolayer MoS<sub>2</sub> films beyond Pt. *ACS Nano* 14: 1707–1714. <https://doi.org/10.1021/acsnano.9b07324>.
- 147** Ye, G., Gong, Y., Lin, J. et al. (2016). Defects engineered monolayer MoS<sub>2</sub> for improved hydrogen evolution reaction. *Nano Letters* 16: 1097–1103. <https://doi.org/10.1021/acs.nanolett.5b04331>.
- 148** Cho, K.H., Seo, H., Park, S., et al. (2020). Uniform, assembled 4 nm Mn<sub>3</sub>O<sub>4</sub> nanoparticles as efficient water oxidation electrocatalysts at neutral pH. *Advanced Functional Materials* 30: 1910424. <https://doi.org/10.1002/adfm.201910424>.
- 149** Alvarez, P.J.J., Chan, C.K., Elimelech, M. et al. (2018). Emerging opportunities for nanotechnology to enhance water security. *Nature Nanotechnology* 13: 634–641. <https://doi.org/10.1038/s41565-018-0203-2>.
- 150** Schiermeier, Q. (2014). Water on tap. *Nature* 510: 327–328.
- 151** Song, Y., Sun, P., Henry, L.L., and Sun, B. (2005). Mechanism for structure and performance controlled preparation of thin film composite membrane via interfacial polymerization. *Journal of Membrane Science* 251: 67–72.
- 152** Song, Y., Liu, F., and Sun, B. (2005). Preparation, characterization, and application of thin film composite nanofiltration membranes. *Journal of Applied Polymer Science* 95: 1251–1256.
- 153** Song, Y. (2000). Nanofiltration thin film composite membranes. PhD thesis. Beijing University of Chemical Technology.
- 154** Inukai, S., Cruz-Silva, R., Ortiz-Medina, J. et al. (2015). High-performance multi-functional reverse osmosis membranes obtained by carbon nanotube-polyamide nanocomposite. *Scientific Reports* 5: 13562. <https://doi.org/10.1038/srep13562>.
- 155** Geng, H., Xu, Q., Wu, M., et al. (2019). Plant leaves inspired sunlight-driven purifier for high-efficiency clean water production. *Nature Communications* 10: 1512. <https://doi.org/10.1038/s41467-019-09535-w>.
- 156** Chen, W., Chen, S., Liang, T., et al. (2018). High-flux water desalination with interfacial salt sieving effect in nanoporous carbon composite membranes. *Nature Nanotechnology* 13: 345–350. <https://doi.org/10.1038/s41565-018-0067-5>.
- 157** Song, Y., Wang, D.K., Birkett, G., et al. (2016). Mixed matrix carbon molecular sieve and alumina (CMS-Al<sub>2</sub>O<sub>3</sub>) membranes. *Scientific Reports* 6: 30703. <https://doi.org/10.1038/srep30703>.

- 158 Khorshidi, B., Thundat, T., Fleck, B.A., and Sadrzadeh, M. (2016). A novel approach toward fabrication of high performance thin film composite polyamide membranes. *Scientific Reports* 6: 22069. <https://doi.org/10.1038/srep22069>.
- 159 Vlassiouk, I.V. (2017). A scalable graphene-based membrane. *Nature Nanotechnology* 12: 1022–1023. <https://doi.org/10.1038/nnano.2017.184>.
- 160 Chen, L., Shi, G., Shen, J., et al. (2017). Ion sieving in graphene oxide membranes via cationic control of interlayer spacing. *Nature* 550: 380–383. <https://doi.org/10.1038/nature24044>.
- 161 Liang, B., Wang, H., Shi, X., et al. (2018). Microporous membranes comprising conjugated polymers with rigid backbones enable ultrafast organic-solvent nanofiltration. *Nature Chemistry* 10: 961–967. <https://doi.org/10.1038/s41557-018-0093-9>.
- 162 Enrico, D., Lidietta, G., and Enrica, F. (2017). *Comprehensive Membrane Science and Engineering*, 2e. Elsevier Science.
- 163 Al-Abri, M., Al-Ghafri, B., Bora, T., et al. (2019). Chlorination disadvantages and alternative routes for biofouling control in reverse osmosis desalination. *NPJ Clean Water* 2: 2. <https://doi.org/10.1038/s41545-018-0024-8>.
- 164 Byun, Y. and Coskun, A. (2015). Bottom-up approach for the synthesis of a three-dimensional nanoporous graphene nanoribbon framework and its gas sorption properties. *Chemistry of Materials* 27: 2576–2583. <https://doi.org/10.1021/acs.chemmater.5b00246>.
- 165 Ye, H., Li, D., Ye, X., et al. (2019). An adjustable permeation membrane up to the separation for multicomponent gas mixture. *Scientific Reports* 9: 7380. <https://doi.org/10.1038/s41598-019-43751-0>.
- 166 Han, Y., Xu, Z., and Gao, C. (2013). Ultrathin graphene nanofiltration membrane for water purification. *Advanced Functional Materials* 23: 3693–3700.
- 167 Keerthi, A., Geim, A.K., Janardanan, A., et al. (2018). Ballistic molecular transport through two-dimensional channels. *Nature* 558: 420–424. <https://doi.org/10.1038/s41586-018-0203-2>.
- 168 Geim, A.K. and Grigorieva, I.V. (2013). Van der Waals heterostructures. *Nature* 499: 419–425. <https://doi.org/10.1038/nature12385>.
- 169 Joshi, R.K., Carbone, P., Wang, C., et al. (2014). Precise and ultrafast molecular sieving through graphene oxide membranes. *Science* 343: 752–754. <https://doi.org/10.1126/science.1245711>.
- 170 Liu, G.P., Jin, W.Q., and Xu, N.P. (2015). Graphene-based membranes. *Chemical Society Reviews* 44: 5016–5030.
- 171 Yang, Q., Su, Y., Chi, C., et al. (2017). Ultrathin graphene-based membrane with precise molecular sieving and ultrafast solvent permeation. *Nature Materials* 16: 1198–1202. <https://doi.org/10.1038/nmat5025>.
- 172 Li, B., Japip, S., and Chung, T.-S. (2020). Molecularly tunable thin-film nanocomposite membranes with enhanced molecular sieving for organic solvent forward osmosis. *Nature Communications* 11: 1198. <https://doi.org/10.1038/s41467-020-15070-w>.

- 173** Mahmoudi, E., Ng, L.Y., Ang, W.L., et al. (2019). Enhancing morphology and separation performance of polyamide 6,6 membranes by minimal incorporation of silver decorated graphene oxide nanoparticles. *Scientific Reports* 9: 1216. <https://doi.org/10.1038/s41598-018-38060-x>.
- 174** Celebi, K., Buchheim, J., Wyss, R.M., et al. (2014). Ultimate permeation across atomically thin porous graphene. *Science* 344: 289–292.
- 175** Dikin, D.A., Stankovich, S., Zimney, E.J., et al. (2007). Preparation and characterization of graphene oxide paper. *Nature* 448: 457–460. <https://doi.org/10.1038/nature06016>.
- 176** Elimelech, M. and Phillip, W.A. (2011). The future of seawater desalination: energy, technology, and the environment. *Science* 333: 712–717.
- 177** Gin, D.L. and Noble, R.D. (2011). Designing the next generation of chemical separation membranes. *Science* 332: 674–676.
- 178** Radha, B., Esfandiari, A., Wang, F.C., et al. (2016). Molecular transport through capillaries made with atomic-scale precision. *Nature* 538: 222–225. <https://doi.org/10.1038/nature19363>.
- 179** Sun, P., Zheng, F., Zhu, M., et al. (2014). Selective trans-membrane transport of alkali and alkaline earth cations through graphene oxide membranes based on cation– $\pi$  interactions. *ACS Nano* 8: 850–859. <https://doi.org/10.1021/nn4055682>.
- 180** Surwade, S.P., Smirnov, S.N., Vlassiuk, I.V., et al. (2015). Water desalination using nanoporous single-layer graphene. *Nature Nanotechnology* 10: 459–464. <https://doi.org/10.1038/nnano.2015.37>.
- 181** Lin, L.-C. and Grossman, J.C. (2015). Atomistic understandings of reduced graphene oxide as an ultrathin-film nanoporous membrane for separations. *Nature Communications* 6: 8335. <https://doi.org/10.1038/ncomms9335>.
- 182** Kim, H.W., Yoon, H.W., Yoon, S.-M., et al. (2013). Selective gas transport through few-layered graphene and graphene oxide membranes. *Science* 342: 91–95. <https://doi.org/10.1126/science.1236098>.
- 183** Li, H., Song, Z., Zhang, X., et al. (2013). Ultrathin, molecular-sieving graphene oxide membranes for selective hydrogen separation. *Science* 342: 95–98. <https://doi.org/10.1126/science.1236686>.
- 184** Koenig, S.P., Wang, L., Pellegrino, J., and Bunch, J.S. (2012). Selective molecular sieving through porous graphene. *Nature Nanotechnology* 7: 728–732. <https://doi.org/10.1038/nnano.2012.162>.
- 185** De Volder, M.F.L., Tawfick, S.H., Baughman, R.H., and Hart, A.J. (2013). Carbon nanotubes: present and future commercial applications. *Science* 339: 535–539. <https://doi.org/10.1126/science.1222453>.
- 186** Sun, P., Wang, K., and Zhu, H. (2016). Recent developments in graphene-based membranes: structure, mass-transport mechanism and potential applications. *Advanced Materials* 28: 2287–2310.
- 187** Seo, D.H., Pineda, S., Woo, Y.C., et al. (2018). Anti-fouling graphene-based membranes for effective water desalination. *Nature Communications* 9: 683. <https://doi.org/10.1038/s41467-018-02871-3>.
- 188** Lee, S.Y., Jung, H., Kim, N.-K., et al. (2018). Mixed copper states in anodized Cu electrocatalyst for stable and selective ethylene production from CO<sub>2</sub>

- reduction. *Journal of the American Chemical Society* 140: 8681–8689. <https://doi.org/10.1021/jacs.8b02173>.
- 189** Yi, Z., Xin-feng, Q., and Zi-li, Z. (2014). Technical analysis and application prospect on resource utilization of carbon dioxide resource technology. *Science Technology & Engineering* 16: 175–183.
- 190** Varela, A.S., Ju, W., Bagger, A., et al. (2019). Electrochemical reduction of CO<sub>2</sub> on metal–nitrogen-doped carbon catalysts. *ACS Catalysis* 9: 7270–7284. <https://doi.org/10.1021/acscatal.9b01405>.
- 191** Hussain, J., Jónsson, H., and Skúlason, E. (2018). Calculations of product selectivity in electrochemical CO<sub>2</sub> reduction. *ACS Catalysis* 8: 5240–5249. <https://doi.org/10.1021/acscatal.7b03308>.
- 192** Ju, W., Bagger, A., Hao, G.-P., et al. (2017). Understanding activity and selectivity of metal–nitrogen-doped carbon catalysts for electrochemical reduction of CO<sub>2</sub>. *Nature Communications* 8: 944.
- 193** Nudelman, R., Alhmoud, H., Delalat, B., et al. (2019). Jellyfish-based smart wound dressing devices containing in situ synthesized antibacterial nanoparticles. *Advanced Functional Materials* 29: 1902783. <https://doi.org/10.1002/adfm.201902783>.
- 194** Madejski, G.R., Briggs, K., DesOrmeaux, J.-P., et al. (2019). Monolithic fabrication of NPN/SiN<sub>x</sub> dual membrane cavity for nanopore-based DNA sensing. *Advanced Materials Interfaces* 6: 1900684. <https://doi.org/10.1002/admi.201900684>.
- 195** Ulubayram, K., Cakar, A.N., Korkusuz, P. et al. (2001). EGF containing gelatin-based wound dressings. *Biomaterials* 22: 1345–1356.
- 196** Madhumathi, K., Sudheesh Kumar, P.T., Abhilash, S., et al. (2010). Development of novel chitin/nanosilver composite scaffolds for wound dressing applications. *Journal of Materials Science: Materials in Medicine* 21: 807–813. <https://doi.org/10.1007/s10856-009-3877-z>.
- 197** Jin, H., Huang, W., Zhu, X. et al. (2012). Biocompatible or biodegradable hyperbranched polymers: from self-assembly to cytomimetic applications. *Chemical Society Reviews* 41: 5986–5997.
- 198** Choueiri, R.M., Galati, E., Thérien-Aubin, H., et al. (2016). Surface patterning of nanoparticles with polymer patches. *Nature* 538: 79–83. <https://doi.org/10.1038/nature19089>.
- 199** Huang, J., Xu, Z., Qiu, W., et al. (2020). Stretchable and heat-resistant protein-based electronic skin for human thermoregulation. *Advanced Functional Materials* 30: 1910547. <https://doi.org/10.1002/adfm.201910547>.
- 200** Nie, Z.H., Petukhova, A., and Kumacheva, E. (2010). Properties and emerging applications of self-assembled structures of inorganic nanoparticles. *Nature Nanotechnology* 5: 15–25.
- 201** Lattuada, M. and Hatton, T.A. (2011). Synthesis, properties and applications of Janus nanoparticles. *Nano Today* 6: 286–308.
- 202** Andala, D.M., Shin, S.H.R., Lee, H.Y., and Bishop, K.J.M. (2012). Templated synthesis of amphiphilic nanoparticles at the liquid–liquid interface. *ACS Nano* 6: 1044–1050.

- 203** Vilain, C., Goettmann, F., Moores, A. et al. (2007). Study of metal nanoparticles stabilised by mixed ligand shell: a striking blue shift of the surface-plasmon band evidencing the formation of Janus nanoparticles. *Journal of Materials Chemistry* 17: 3509–3514.
- 204** Jackson, A.M., Myerson, J.W., and Stellacci, F. (2004). Spontaneous assembly of subnanometre ordered domains in the ligand shell of monolayer-protected nanoparticles. *Nature Materials* 3: 330–336.
- 205** Bao, C., Tang, S., Wright, R.A.E., et al. (2014). Effect of molecular weight on lateral microphase separation of mixed homopolymer brushes grafted on silica particles. *Macromolecules* 47: 6824–6835. <https://doi.org/10.1021/ma501474m>.
- 206** Goto, Y., Yanagi, I., Matsui, K. et al. (2016). Integrated solid-state nanopore platform for nanopore fabrication via dielectric breakdown, DNA-speed deceleration and noise reduction. *Scientific Reports* 6: 31324. <https://doi.org/10.1038/srep31324>.
- 207** Waugh, M., Briggs, K., Gunn, D., et al. (2020). Solid-state nanopore fabrication by automated controlled breakdown. *Nature Protocols* 15: 122–143. <https://doi.org/10.1038/s41596-019-0255-2>.
- 208** Goto, Y., Akahori, R., Yanagi, I., and Takeda, K.-i. (2020). Solid-state nanopores towards single-molecule DNA sequencing. *Journal of Human Genetics* 65: 69–77. <https://doi.org/10.1038/s10038-019-0655-8>.
- 209** Li, J., Zhang, W., Song, Y. et al. (2016). Template transfer nanoimprint for uniform nanopores and nanopoles. *Journal of Nanomaterials* 2016: 9354364.
- 210** Cao, K., Jiang, Z., Zhao, J., et al. (2014). Enhanced water permeation through sodium alginate membranes by incorporating graphene oxides. *Journal of Membrane Science* 469: 272–283. <https://doi.org/10.1016/j.memsci.2014.06.053>.
- 211** Zhou, K.G., Vasu, K.S., Cherian, C.T., et al. (2018). Electrically controlled water permeation through graphene oxide membranes. *Nature* 559: 236–240. <https://doi.org/10.1038/s41586-018-0292-y>.
- 212** Zhao, C., Nie, S., Tang, M., and Sun, S. (2011). Polymeric pH-sensitive membranes—a review. *Progress in Polymer Science* 36: 1499–1520.
- 213** Liu, Z., Wang, W., Xie, R. et al. (2016). Stimuli-responsive smart gating membranes. *Chemical Society Reviews* 45: 460–475.
- 214** Nair, R.R., Wu, H.A., Jayaram, P.N. et al. (2012). Unimpeded permeation of water through helium-leak-tight graphene-based membranes. *Science* 335: 442–444.
- 215** Abraham, J., Vasu, K.S., Williams, C.D., et al. (2017). Tunable sieving of ions using graphene oxide membranes. *Nature Nanotechnology* 12: 546–550. <https://doi.org/10.1038/nnano.2017.21>.
- 216** Gao, Y., Song, J., Li, S., et al. (2016). Hydrogel microphones for stealthy underwater listening. *Nature Communications* 7: 12316. <https://doi.org/10.1038/ncomms12316>.
- 217** Fish, F.E. and Kocak, D.M. (2011). Biomimetics and marine technology: an introduction. *Marine Technology Society Journal* 45: 8–13.
- 218** Becker, G. and Gudesen, A. (2000). Passive sensing with acoustics on the battlefield. *Applied Acoustics* 59: 149–178.

- 219 Asadnia, M., Kottapalli, A.G.P., Shen, Z.Y. et al. (2013). Flexible and surface-mountable piezoelectric sensor arrays for underwater sensing in marine vehicles. *IEEE Sensors Journal* 13: 3918–3925.
- 220 Sanchez, A., Blanc, S., Yuste, P. et al. (2012). An ultra-low power and flexible acoustic modem design to develop energy-efficient underwater sensor networks. *Sensors* 12: 6837–6856.
- 221 Xu, J., Headings, L.M., and Dapino, M.J. (2015). High sensitivity polyvinylidene fluoride microphone based on area ratio amplification and minimal capacitance. *IEEE Sensors Journal* 15: 2839–2847.
- 222 Zhou, Q., Zheng, J.L., Onishi, S. et al. (2015). Graphene electrostatic microphone and ultrasonic radio. *Proceedings of the National Academy of Sciences of the United States of America* 112: 8942–8946.
- 223 Polcawich, R.G., Scanlon, M., Pulskamp, J., et al. (2003). Design and fabrication of a lead zirconate titanate (PZT) thin film acoustic sensor. *Integrated Ferroelectrics* 54: 595–606. <https://doi.org/10.1080/10584580390259010>.
- 224 Zigoneanu, L., Popa, B.I., and Cummer, S.A. (2014). Three-dimensional broadband omnidirectional acoustic ground cloak. *Nature Materials* 13: 352–355.
- 225 Zhu, J., Chen, T., Liang, Q., et al. (2015). A unidirectional acoustic cloak for multilayered background media with homogeneous metamaterials. *Journal of Physics D: Applied Physics* 48: 305502. <https://doi.org/10.1088/0022-3727/48/30/305502>.
- 226 Song, X., Chen, T., Zhu, J. et al. (2019). Broadband acoustic cloaking and disguising with full-range incident angles based on reconfigurable metasurface. *International Journal of Modern Physics B* 33: 1950273. <https://doi.org/10.1142/S0217979219502734>.
- 227 Nohara, S., Wada, H., Furukawa, N., et al. (2003). Electrochemical characterization of new electric double layer capacitor with polymer hydrogel electrolyte. *Electrochimica Acta* 48: 749–753.
- 228 Keplinger, C., Sun, J.-Y., Foo, C.C., et al. (2013). Stretchable, transparent, ionic conductors. *Science* 341: 984–987. <https://doi.org/10.1126/science.1240228>.
- 229 Wen, X.-Y., Liu, Z., Wang, J., et al. (2019). Nanocomposite hydrogels with optic-sonic transparency and hydroacoustic-sensitive conductivity for potential antiscouting sonar. *ACS Applied Materials & Interfaces* 11: 20386. <https://doi.org/10.1021/acsami.9b04463>.
- 230 Li, S., Zheng, J., Yan, J., et al. (2018). Gate-free hydrogel-graphene transistors as underwater microphones. *ACS Applied Materials & Interfaces* 10: 42573–42582. <https://doi.org/10.1021/acsami.8b14034>.
- 231 Zhou, Y., He, B., Yan, Z., et al. (2018). Touch locating and stretch sensing studies of conductive hydrogels with applications to soft robots. *Sensors* 18: 569. <https://doi.org/10.3390/s18020569>.
- 232 Zhang, X., Sheng, N., Wang, L., et al. (2019). Supramolecular nanofibrillar hydrogels as highly stretchable, elastic and sensitive ionic sensors. *Materials Horizons* 6: 326. <https://doi.org/10.1039/C8MH01188E>.